

From the Department of Surgical Sciences, Section of Urology and
the Department of Laboratory Medicine, Division of Medical
Engineering, Karolinska Institutet, Stockholm, Sweden

THERAPEUTIC APPLICATIONS OF ACOUSTIC AND ELECTROMAGNETIC ENERGY

Vilhelm Ekstrand, MSc, Lic



Stockholm 2005

All previously published papers were reproduced with permission from the publisher.

Published and printed by Karolinska University Press

Box 200, SE-171 77 Stockholm, Sweden

© Vilhelm Ekstrand, 2005

ISBN [91-7140-126-1]

ABSTRACT

This thesis focuses on techniques based on electromagnetic and acoustic energy for treatment of a variety of diseases, including development of new techniques as well as improvement and evaluation of existing techniques. The subjects treated are:

Provocation of heat generated thrombi in pigs. A bipolar RF-catheter was introduced in the vessel of interest where 6 W of RF-energy was applied through the catheter for 30 seconds. Subsequently the vessel was occluded for 15 minutes. With this protocol, 100 % (n = 11) of the vessels were occluded with an associating thrombotic mass completely filling the entire lumen. Using a static dose may cause severe or insufficient damage to the vessel wall because of varying blood flow in the in-vivo situation. The behaviour of the electrical impedance during exposure in different tissues was therefore studied to create a more standardised injury to the vessel wall independent of blood flow.

Trans Urethral Microwave Thermotherapy (TUMT), with the ECP-system. Between 1991 and 1999, 371 patients were treated with TUMT at Karolinska Hospital, Sweden. Seventy-six percent of the patients subjectively benefited from the TUMT treatment and 22 % judged they were fully cured. IPSS and Quality of Life score decreased approximately 40 % and 30 % respectively. Forty-one percent of the patients with CAD (cathéter à demeure) before the treatment became permanently or temporarily catheter free after the treatment. Furthermore, the cross-correlation between output power and rectal temperature was studied during 15 in-vivo treatments to assess if catheter dislocations could be automatically detected as a change in the cross-correlation. The sampled in-vivo data showed no detectable cross correlation, preventing the realisation of this automatic technique.

Variation in electrical tissue admittivity after exposure to acoustic energy. The effects of three modes of acoustic energy on in-vitro electrical admittivity were studied. Thirty-four muscle tissue samples were irradiated with either extra corporeal shock wave lithotripsy (ESWL) or high intensity focused ultrasound (HIFU) in pulsed or continuous wave. Significant changes in magnitude of admittivity were detected only during continuous HIFU when temperatures over 44°C were generated. The admittivity decreased by 35 % during these protocols. The phase angle of impedivity increased during all our protocols. The increase was approximately 50-70 % depending on the temperature elevation and the mode of delivery. We conclude that both thermal and non-thermal effects have an impact on the phase angle of the target tissue.

Treatment of breast cancer with a cooled monopolar RF-system. Initially, a complete RFA-system was developed on which the power distribution around the needle was mapped. Subsequently, treatment on in-vitro breast tissue with tumour was performed, showing that ductal breast cancer was well suited for RF-ablation. Interestingly, thin tumour strips extending from the core tumour were also killed. The surrounding fat was however unaffected. Hence, the heat pattern appears to be drawn to the tumour. The origin of this focusing effect was studied using Finite Element Method (FEM) analysis. The dissimilarity of mainly the electrical properties in tumour and fat is capable of focusing the heating to the tumour. The degree of this differentiating effect depends on tumour shape and placement relative to the electrode. However, the observed differentiating effect between tumour and fat in the in-vitro studies were more pronounced, indicating that additional effects might be involved in the tumour targeting.

LIST OF PUBLICATIONS

- I. **Provocation of Heat Generated Arterial Thrombi in Pigs**
V Ekstrand, H Berglund and H Wiksell
Physica Medica 2001, 17: 135-140
- II. **Long-term Clinical Outcome of Trans Urethral Microwave Thermotherapy (TUMT) 1991-1999 at Karolinska Hospital, Sweden**
V Ekstrand, S Westermark, H Wiksell, B Bergman and K Cronwall
Scand J Urol Nephrol 2002, 36: 113-118
- III. **Variation in Electrical Tissue Admittivity after Exposure to Different Types of Acoustic Energy, an In-vitro Study**
V Ekstrand and H Wiksell
Physica Medica 2004, 20: 13-18
- IV. **The Influence of Tumour Properties on Lesion Shape During Radio Frequency Ablation in Breast Tissue: a FEM Study**
V Ekstrand, H Wiksell, I Schultz, B Sandstedt, S Rotstein and A Eriksson
Sent to journal

The work in this thesis was supported and founded by VINNOVA, Comair AB and VibraTech AB, SWEDEN

CONTENTS

1	Introduction	5
2	Acoustic energy	6
2.1	Wave equation	6
2.2	Reflection and transmission at interfaces	8
2.3	Superposition	8
2.4	Absorption	9
2.5	Biological effects	9
2.6	HIFU	10
2.7	ESWL	10
3	Electromagnetic energy	12
3.1	RF	13
3.2	Measuring electrical properties in tissue	15
3.3	Microwaves, TUMT	16
4	Thermotherapy	19
5	Finite element analysis (FEM)	23
6	Microwave energy, evaluation and improvement of the TUMT technique	26
6.1	Long-term clinical outcome of TUMT using the ECP-system	27
6.2	Automatic detection of catheter dislocation	29
6.3	Conclusion and future work	31
7	Development of RF-techniques	33
7.1	RFA treatment of breast tumours	33
7.2	Provocation of blood clots	41
7.3	Conclusion and future work	43
8	Acoustic techniques	45
8.1	HIFU treatment of tumours	45
8.2	The effects of acoustic energy on electrical admittivity	45
8.3	Conclusion and future work	48
9	Acknowledgements	49
10	References	51

LIST OF ABBREVIATIONS

BPH	Benign Prostatic Hyperplasia
CAD	Catheter A Demeure
ESWL	Extra corporeal Shock Wave Lithotripsy
FEM	Finite Element Method
HIFU	High Intensity Focused Ultrasound
IPSS	International Prostate Symptom Score
QL	Quality of Life
RFA	Radio Frequency Ablation
RF	Radio Frequency
SAR	Specific Absorption Rate
SPTA	Spatial Peak Temporal Average
SPTP	Spatial Peak Temporal Peak
TUMT	Trans Urethral Microwave Thermotherapy
TUR-P	Trans Urethral electro Resection of the Prostate

1 INTRODUCTION

Electromagnetic and acoustic energy is extensively used in modern health care, both for therapeutic and diagnostic purposes [1]. This thesis discusses some of the therapeutic applications. The therapeutic effect of the discussed applications originates from absorption of energy, resulting in thermal or micro-mechanical injury.

The trend in modern therapy is the development of less invasive methods. These techniques have many financial as well as medical advantages such as reduced mortality and morbidity rates, reduced treatment duration, ability to perform therapy even when patients are in poor medical condition and keep the procedure on an outpatient basis with minimal convalescence needs.

The discussed energy forms are described with well-known physical equations. However when transmitted through tissue, complicated non-linear and time-variant phenomena often occur. The nature of these phenomena is often not fully known and can thus not be fully described in fundamental equations. Therefore, a combination of basic theoretical studies with empirical studies is necessary to successfully avoid or even use the non-linearities to our own advantage. Many methods not fully applicable today will in the future become possible when advanced feed forward and feed back regimes etc. are developed.

This thesis focuses on five different applications of acoustic and electromagnetic energy. Improvements and evaluation of older methods as well as development of new techniques were undertaken in the studies. The applications discussed are:

1. Transurethral Microwave Thermotherapy, TUMT

Treatment of benign prostatic hyperplasia, BPH, by inducing a thermal lesion in the prostate through an intra-urethral catheter system.

2. Provocation of heat-generated thrombi

An intra-arterial bipolar RF catheter initiates the coagulation cascades.

3. Treatment of breast cancer with a cooled monopolar RFA-system

A treatment needle electrode is inserted into the tumour. The current from the needle induces heat lesions which kill the tumour.

4. Extra Corporeal Shock Wave Lithotripsy (ESWL)

Externally applied focused acoustic shockwaves fragment kidney stones.

5. High Intensity Focused Ultrasound (HIFU)

A non-invasive technique to heat tissues or disrupt biological structures by cavitation phenomena.

2 ACOUSTIC ENERGY

The behaviour of acoustic energy is described by wave theory. Important wave characteristics are superposition, reflection and absorption. The wave energy is transported by motion of particles within the medium from their steady state position, i.e. no net transport of material. The propagation of the wave causes compressions and rarefactions of the medium. This, in turn generates a pressure wave propagating with the mechanical wave. The propagating waves can be transversal and/or longitudinal depending on whether the particles vibrate perpendicularly to or along the direction of the wave propagation respectively. Transversal waves are created for example at tissue interfaces but are of minor importance for this work. Consequently, only longitudinal waves will be discussed henceforth. The behaviour of the wave is similar to the behaviour of mass particles connected to each other by springs, figure 1, i.e. the forces between the particles are represented by springs for a better intuitive understanding. The physical form of the wave is dependent on the initial disturbance of particles, seen in the upper left corner of figure 1, and the acoustic properties of the medium, represented by the mass of the particles and the spring constants.

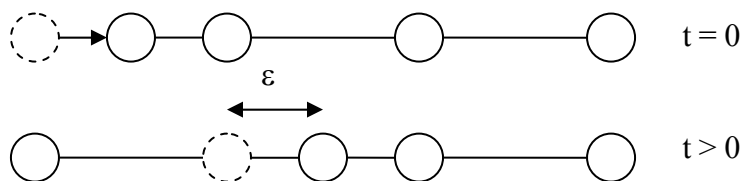


Figure 1. Shows the particles and their corresponding interacting forces here represented by springs. The initial positions of the dislocated particles are shown as dotted circles. ϵ is the dislocation of the particles from their steady state position (m).

2.1 WAVE EQUATION

The propagation of acoustic energy can be described by wave theory since the equilibrium equation of forces acting on the medium results in a wave equation. Mainly two types of forces are acting on the volume element in figure 2, described by Hooke's law and Newton's second law.

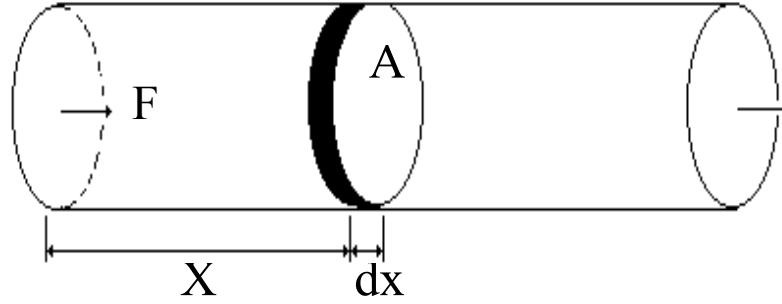


Figure 2. A planar wave is propagating in the tube where we look at the forces acting on a volume element with cross section area A and thickness dx.

Hooke's law corresponds to the spring forces in figure1:

$$F_x = -AK \frac{d\xi}{dx} = -AK\xi' \quad \text{equation 1)}$$

where F is the force acting on the cross section A in figure 2, K is the bulk modulus of the medium, ξ is the dislocation of the medium and x is the spatial coordinate along the propagation. The resulting force on the thin volume element is:

$$dF_x = F_x(x+dx) - F_x(x) = \frac{-AK(\xi'(x+dx) - \xi'(x))}{dx} dx = -AK \frac{\partial^2 \xi}{\partial x^2} \cdot dx \quad \text{equation 2)}$$

Newton's second law corresponds to the forces acting on accelerated or retarded mass particles that for the volume element results in:

$$dF_x = m \cdot a = \rho_0 \cdot A \cdot dx \cdot \frac{d^2 \xi}{dt^2} \quad \text{equation 3)}$$

where m is the mass of the volume element, ρ_0 is the density of the medium before sonication and t is the time coordinate. The sum of all forces on any mass element is always zero, resulting in equation 4:

$$-\frac{\partial^2 \xi}{\partial x^2} + \frac{\rho_0}{K} \cdot \frac{d^2 \xi}{dt^2} = -\frac{\partial^2 \xi}{\partial x^2} + \frac{1}{v^2} \cdot \frac{d^2 \xi}{dt^2} = 0 \quad \text{equation 4)}$$

where ρ_0/K is substituted for v. The solution to the wave equation is:

$$\xi(x,t) = F(t \pm x/v) = \xi_{\max} \cdot \text{Sin}(\omega(t \pm x/v)) \quad \text{equation 5)}$$

where F is any derivable function travelling in both directions along the x coordinate. Hence, v is the propagation speed of the wave which is a material constant that differs from the particle speed, i.e. the first time derivative of the dislocation. Therefore, quite beautifully, the solution to the wave equation is a dislocation function F travelling in both directions, with speed v, to account for any reflections along the propagation path. The excitation of the first particle layer is often sinusoidal due to resonances in the transducer, which produces a sinusoidal wave, equation 5.

The dislocation wave must create a corresponding pressure wave, as discussed above. What is the relationship between these two wave properties? If we take a look at Hooke's law again and divide both sides with A , we have the definition of pressure on the left side, equation 6. By calculating the derivative of the dislocation with respect to x and t , using the wave function in equation 5, the relation between the derivatives is obtained. In equation 6 the spatial derivative is substituted by the time derivative, using this relation.

$$P = -K \frac{\partial \xi}{\partial x} = -\rho_0 \cdot v^2 \cdot \frac{\partial \xi}{\partial x} = \rho_0 \cdot v \cdot \frac{d\xi}{dt} = \rho_0 \cdot v \cdot u = Z \cdot u$$

equation 6)

A relation between the pressure and the particle speed in the wave is now established. The constant Z is called acoustic impedance and describes the relation between pressure and particle speed u , exactly as Ohm's law describes the relation between voltage and current. Furthermore, the energy flow through a unit area is defined as the acoustic intensity of the wave, equation 7.

$$I = \frac{P^2}{Z} = Z \cdot u^2$$

equation 7)

2.2 REFLECTION AND TRANSMISSION AT INTERFACES

At the interface between tissues with dissimilar acoustic impedance part of the energy is reflected. The remaining wave energy is of course transmitted into the new medium. The part of the incident energy that is reflected is described by the reflection coefficient R , equation 8. The value of R is dependent on the relative difference in acoustic impedance.

$$R = \left[\frac{Z_1 - Z_2}{Z_1 + Z_2} \right]^2$$

equation 8)

Hence, the intensity of the reflected part is determined by the reflection coefficient R and the incident intensity. In diagnostic ultrasound the reflected energy from the tissue interfaces are used to produce the visual representation the body. For more complicated cases where the incident wave is not perpendicular to the reflecting interface, the angle of the incident and reflected wave are equal whereas the angle of the transmitted wave is dependent on the quota of the medium velocities and the incident angle, described by Snell's law.

2.3 SUPERPOSITION

Another important wave characteristic is superposition which states that the resulting wave is the sum of all waves propagating in the same volume. Due to reflection the wave can interact with itself creating standing waves. This is the case in for example an organ pipe or an ultrasound aspiration hand piece, which are half wave resonators.

2.4 ABSORPTION

Absorption of energy along the wave path is inevitable due to the friction forces acting on the oscillating particles. The change in intensity along the propagation path, i.e. the absorption, is proportional to the intensity, equation 9.

$$\frac{dI}{dx} = -\mu \cdot I \quad \text{equation 9)}$$
$$I(x) = I(0) \cdot e^{-\mu \cdot x} = I(0) \cdot e^{-\mu_0 \cdot f \cdot x}$$

where μ is the absorption coefficient (1/m). The solution to the differential equation is an exponential function. μ increases with the oscillation frequency. Consequently, the intensity rapidly decreases with both increasing penetration depth x and oscillation frequency f . Often a trade off between penetration depth and other frequency dependent parameters, such as resolution in the imaging applications or appropriate focusing in the therapeutic applications, is necessary.

2.5 BIOLOGICAL EFFECTS

The discussed therapeutic effects of acoustic energy in this thesis are thermal and mechanical phenomena [2-3]. Thermotherapy is the most straight forward therapeutic mechanism. Due to viscous friction between particles temperature elevation occurs along the propagation path as energy is absorbed from the wave. Cavitation on the other hand is a very aggressive mechanical phenomenon occurring at high intensities [4]. Cavities are created around irregularities in the medium because the medium fails to withstand the created high under pressure. These bubbles start to oscillate with the sound field, absorb energy and increase in size due to rectified diffusion up to its resonance frequency where they begin to oscillate more violently and cause micro streaming of the fluid around the bubbles. The resonance diameter at 1MHz is $3.5\mu\text{m}$ [5]. At even higher intensities transient cavitation starts to occur. These oscillations are highly non-linear and expand and collapse during one oscillation cycle. The collapse of these bubbles emit shockwaves of acoustic energy that are capable of creating free radicals and putting immense mechanical stress on the target region. Our group have found that such phenomena can destroy blood clots from human blood [6] and cell structures as we will see later in this thesis. The cavitation thresholds and thus also the therapeutic effects are highly dependent on the pressure, gas balance, inhomogenities, temperature and the density of the target. The stresses caused by particle movements without cavitation phenomena are considered insignificant. For a beam in tissue with frequency 1MHz and intensity $100\text{W}/\text{cm}^2$ the displacement is $0.18\mu\text{m}$ over a length of 0.75mm (half wave length) [5].

2.6 HIFU

High Intensity Focused Ultrasound (HIFU) is mainly used for therapeutic purposes. Researchers have studied this promising non-invasive technique since the mid 1940's without any major breakthrough [7-13]. Two of the major drawbacks are varying target alteration due to non-linearities and high attenuation partly due to shielding [14]. Thus, proper feedback parameters are needed to assess the target alteration. The shielding effect is created by the cavitation bubbles which reflect subsequently incoming sound from the target. This effect increases with exposure time and intensity and is time variant i.e. able to deposit a bubble memory. Thus, the attenuation might stay high for long periods even if the ultrasound has been completely turned off. In the in-vivo situation the relaxation time for this process is highly dependent on the perfusion. Another factor that seems to be of importance is the frequency spectra of the acoustic excitation. Wiksell [15] has shown that a broad band frequency spectrum significantly decreases the attenuation created by the cavitation bubbles.

Both mechanical and thermal effects can be produced depending on the wave form created by the power source. Our test equipment uses a piezoelectric technique to create the high intensity ultrasound. Piezoelectric ceramic materials change dimensions when a voltage is applied over it. A piezoelectric transducer is thus capable of transforming electric energy into acoustic energy.

Our experimental transducer is made of fifteen spherically curved piezoelectric ceramic plates glued to spherically shaped hard neoprene foam resting on an aluminium body. The theoretical gain G due to the focusing of the transducer is 7000. The -6 db focus volume is approximately 10 mm^3 . The true acoustic power at the focus can be calculated by measuring the radiation pressure force, caused by the momentum change occurring at interfaces where acoustic energy is absorbed or reflected. The radiation force in our studies was measured with a precision digital balance, mounted on a flat circular reflector immersed in water at the focal point. The electrical acoustic conversion efficiency to the focus of this system at 10W and 70W sine wave was approximately 50 % in degassed water.

2.7 ESWL

Extra corporeal Shock Wave Lithotripsy (ESWL) has since the 1980's been used as the standard treatment for patients with kidney stones. The method is fully non-invasive. A highly non-linear acoustic wave is created by an electro-hydraulic or a piezoelectric method. Our equipment uses the electro-hydraulic method, Lithocut C 3000, Comair AB, SWEDEN [16-21].

A pulse-forming network (PFN) consisting of distributed capacitances and inductances is charged with a high dc-voltage of 12 to 30 kV. The PFN is then rapidly discharged by a trigger-event into an electrode gap placed in saline water at the primary focus of an ellipsoidal reflector, figure 3. The saline water in the plasma-gap is consequently explosively vaporised, giving rise to an isotropically radiating positive high-pressure pulse with very short

temporal duration (half magnitude time width 250-300 ns) and an extremely fast rise time (approx. 20 ns). The pulse is reflected, non-inverted, via the truncated rotational symmetric ellipsoidal aperture (diameter 230 mm, focal-focal distance 230 mm), that focuses the acoustic energy into the secondary target focus. The focus is hourglass shaped with a - 6dB intensity or half pressure volume of 16×7 mm. The frequency spectrum displays a characteristic broadband behaviour because of the very fast rise time. Hence, there are significant differences between the piezoelectric and the electro hydraulic techniques regarding both wave duration and frequency spectrum. This might be the explanation for the excellent transmission properties during the latter ESWL technique. However the short sonication time is likely to abate most of the effect from the ultrasound itself on its own attenuation.

The fragmenting mechanism is thought to originate from cavitation phenomena inside the cavities of the spongy stone and mechanical wearing at the stone water interface due to the positive interference between incoming and reflected waves. The therapeutic results are also highly dependent on both the concentration of dissolved gases [22] and aperture size [23]. The latter, probably due to the better focusing effect for larger aperture diameters.

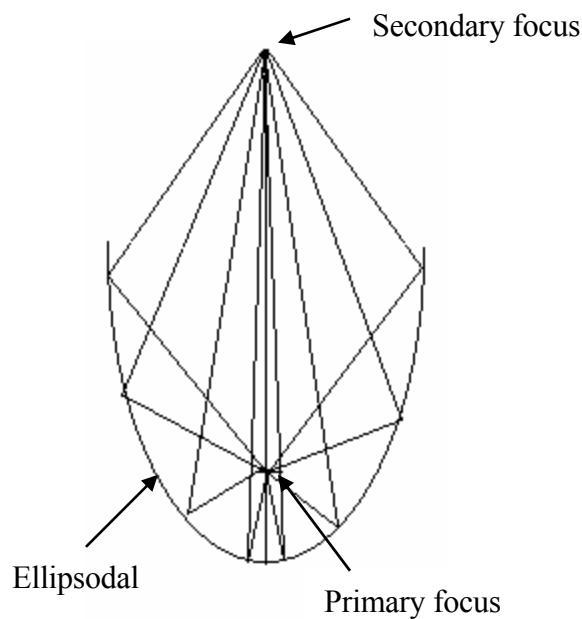


Figure 3. Describes the function of the used focusing ellipsoidal. The diameter and the focal-focal distance are 230 mm.

3 ELECTROMAGNETIC ENERGY

The postulated governing equations for electromagnetic energy are called Maxwell's equations, equations 10-13. These four equations, presented by Maxwell himself in 1864, describe almost all of the existing electromagnetic effects in one powerful set. The work was based on discoveries by Faraday and others and is based on the presumption that charges are always conserved. The equations can be applied to any inertial reference frame and are linear. They are functional also for non-homogenous, non-linear and anisotropic materials (dependent on direction).

$$1. \nabla \cdot \bar{E} = \frac{\rho}{\epsilon_0} \quad \text{Gauss' law, equation 10)}$$

$$2. \nabla \times \bar{E} = -\frac{\partial \bar{B}}{\partial t} \quad \text{Faraday's law, equation 11)}$$

$$3. \nabla \cdot \bar{B} = 0 \quad \text{equation 12)}$$

$$4. \nabla \times \bar{B} = \frac{1}{c^2} \left[\frac{\partial \bar{E}}{\partial t} + \frac{\bar{j}}{\epsilon_0} \right] \quad \text{Ampere's circuital law, equation 13)}$$

E is the electric field (V/m), ρ is the total charge density i.e. both free and bound charges, ϵ_0 is the dielectric permittivity for free space (F/m), B is the magnetic flux density (Wb/m² or Tesla), c is the speed of light (m/s²) and j is the total current density of both bound and free charges (A/m²). Vector variables have both a magnitude and a direction property and are presented with an over-bar. One remarkable feature of these equations is that fields created by accelerating charges can leave the source and travel alone through empty space. In the near field where the distance to the source is $\ll \lambda$, the E and B field are independent of each other, meaning it is possible that only electrical fields exist. In the far field, the fields are entangled (interdependent) and the energy is explained by wave and radiation theory. The wave properties of for example the E field can be identified by using the vector identity in equation 14 on equation 11.

$$\nabla \times \nabla \times \bar{E} = \nabla(\nabla \cdot \bar{E}) - \nabla^2 \bar{E} \quad \text{equation 14)}$$

$$\nabla(\nabla \cdot \bar{E}) - \nabla^2 \bar{E} = -\frac{d}{dt} \nabla \times \bar{B} = -\frac{1}{c^2} \frac{d}{dt} \left(\frac{d\bar{E}}{dt} + \frac{\bar{j}}{\epsilon_0} \right) \quad \text{equation 15)}$$

$$\nabla^2 \bar{E} - \frac{1}{c^2} \frac{d^2 \bar{E}}{dt^2} = 0 \quad \text{equation 16)}$$

In equation 15 the curl and time derivative are interchanged, which is correct if the spatial and time dependence are separable. Subsequently, the curl of B in equation 13 is inserted on the right hand side of equation 15. If we look at a "medium" with $j=0$ and $\rho=0$, as in empty space, equation 16 is obtained. Interestingly enough, this is almost the same equation as the wave equation for acoustic energy, equation 4. Hence the fields in Maxwell's equations can be described by wave theory, where the waves propagate with speed c. Important wave theory concepts such as reflection and standing

waves can therefore also be applied to electromagnetic waves. Due to the fact that the divergence of a curl always is zero, the divergence of the right hand side of equation 13 is zero, resulting in equation 17.

$$\nabla \cdot \frac{\partial \bar{E}}{\partial t} = \frac{d}{dt} (\nabla \cdot \bar{E}) = \frac{1}{\epsilon_0} \cdot \frac{d\rho}{dt} = -\nabla \cdot \frac{\bar{J}}{\epsilon_0} \quad \text{equation 17)}$$

Hence, we can see that the equations predict the conservation of charge, i.e. the current through a closed surface is the same as the change of charges inside said surface.

3.1 RF

RF-energy is widely used in modern health care, in for example electrosurgical applications. One promising upcoming technique is tumour ablation that up to date mainly has been used for research purposes. Due to the operating frequency of our RF-equipment the wavelength is several times larger than the target region. For example, a frequency of 1.5 MHz results in a propagation velocity in muscle and fat tissue of 9.4×10^6 m/s and 6.0×10^7 m/s respectively [24]. Consequently, the corresponding wavelengths at the same frequency will be 6.3 m and 40.4 m respectively. Hence, we are clearly in the near region where a quasi static assumption can be made, i.e. the electrical potential is approximately in phase over the whole target region.

The energy is predominantly dissipated through resistive heating due to the relatively high ion mobility at these frequencies. Further, the magnetic field is considered to be negligible. For spherical current density the two terms on the right hand side in equation 13 cancel out. The operating frequency of RFA devices is sufficiently high not to cause any nerve stimulation and pain [25], because 10 kHz is thought of as the upper limit for stimulation. The stimulation threshold increases drastically with frequency. Nevertheless, electro surgery is sometimes accompanied with stimulation of nerves and muscles, despite the high frequency [26]. This is thought to originate from local low frequency currents generated by demodulation or rectification processes in the tissue [27].

The absorption and penetration of the energy are mostly dependent on the geometry of the conducting electrode. Therefore, the electrode size and shape may be chosen independently of frequency for optimised absorption distribution. Assuming a quasi static situation, the force and consequently also the acceleration acting on a charge is parallel to the E-field, due to the negligible magnetic field. The direction of the current density should therefore be parallel to the E-field, equation 18.

$$\begin{aligned}\bar{E} &= \begin{bmatrix} \rho_x & 0 & 0 \\ 0 & \rho_y & 0 \\ 0 & 0 & \rho_z \end{bmatrix} \cdot \bar{J} \\ \bar{J} &= \begin{bmatrix} \sigma_x & 0 & 0 \\ 0 & \sigma_y & 0 \\ 0 & 0 & \sigma_z \end{bmatrix} \cdot \bar{E}\end{aligned}\quad \text{equation 18)}$$

where σ is the admittivity (S/m) and ρ the impedivity (Ωm) of the medium. The impedivity and admittivity of a homogenous material are constant and independent of sample volume. The tensor representation of the admittivity and impedivity in equation 18 is due to the fact that the properties can be dissimilar in different directions. For example muscle tissue properties differ along and orthogonal to the muscle fibres. However, admittivity and impedivity are often considered to be the same in all directions (isotropic). Both σ_i and ρ_i are complex properties that represent both the phase difference and the quota between the current density and the electric field. The phase angle of impedivity and admittivity has the same magnitude, but has opposite signs. The real part of the admittivity is called conductivity. The power density absorbed at each point is the electric field multiplied with the current density.

$$p = \bar{E} \cdot \bar{J} = \frac{\bar{J}^2}{|\sigma|} \cos \alpha = |\sigma| \cdot \bar{E}^2 \cos \alpha \quad \text{equation 19)}$$

where p is the power density (W/m^3), α is the phase angle of σ ($^\circ$, rad) and sidebars represent the magnitude of the complex properties. The phase-shift during RFA treatment is approximately zero. Hence only the real part of the admittivity, called conductivity is henceforth used. The electric potential in a volume can be solved using Laplace's equation:

$$\nabla \cdot [\sigma \cdot \nabla V] = \nabla \cdot [\sigma \cdot \bar{E}] = \nabla \cdot \bar{J} = 0 \quad \text{equation 20)}$$

where V is the electrical potential (V) and σ is the conductivity (S/m). This equation is similar to equation 1 but relates to the current density instead of the electric field. It specifies that the current flow into a closed surface must always be zero. Since the change of charge inside a closed surface is assumed to be zero without a current source, the current into said surface must also always be zero, equation 17. The solution to equation 20 is used to calculate the power density.

RF devices cause thermal elevation in the target region by ion agitation, which is converted by means of friction into heat. The current is induced by an applied voltage between two electrodes. The current paths between the electrodes are distributed in a manner that minimises the total resistance, which is a property of equation 20. The RF-energy can be applied using a monopolar or a bipolar regime. The bipolar regime uses two active electrodes where temperature elevation occurs at both electrodes. The monopolar regime uses one treatment electrode (active) and one indifferent (passive) electrode. Therapeutic temperature elevation occurs only at the treatment electrode due to the relatively higher current density caused by the

much smaller electrode area. The total current through each closed surface enclosing one of the electrodes always equals the total current from the generator, independent of surface size. Hence, the heating will be demarcated to the region close to the active electrode where this surface is small and the current density is high. For a postulated point source the absorbed power at each point at distance r from the source is:

$$p = \frac{\bar{J}^2}{\sigma} = \frac{I^2}{\sigma} \cdot \frac{1}{A^2} = \frac{I^2}{\sigma} \left(\frac{1}{4\pi \cdot r^2} \right)^2 \quad \text{equation 21)}$$

where I is the current (A), A is the spherical area enclosing the active electrode (m^2) and r is the radius of the spherical area (m). Consequently, the absorbed power density decreases rapidly with increasing distance to the electrode. During the initial phase of all tissue protocols, the electrical impedance between the electrodes decrease as temperature increases over time. This is explained by the temperature dependent conductivity of the tissue. However, when the tissue temperature reaches 100°C the formation of small gas bubbles occur, due to tissue phase transformation, at the needle interface. The created gas bubbles function as electrical insulation which alters the effective electrode area and further increases the current density and temperature. This avalanche-like phenomenon ultimately insulates the electrode from the tissue and the heating often ceases non-reversibly. This electrode insulation phenomenon limits the ablation volume to approximately 16 mm in diameter in muscle or liver [28], due to the limited output power. Several techniques have been used to increase the necrotic region; for example multiprobe needles [29], saline injected needles [30] and internally cooled needles [31]. These techniques change the electrode area, increase the tissue conductivity or cool the warmest region respectively to avoid insulation and be able to increase the output power and lesion volume.

3.2 MEASURING ELECTRICAL PROPERTIES IN TISSUE

The use of electrical tissue parameters in clinical practice has so far been fairly sparse, with a few exceptions such as total body composition analysis [32]. Other potential techniques are electrical impedance tomography (EIT) [33] and detection of skin cancer [34-36], which to date are mainly used for research purposes. We have monitored changes in electrical parameters after thermotherapy, HIFU and ESWL to assess if these can serve as indicators of the therapeutic result. Jossinet et al have demonstrated an intra-operative impedance method to evaluate the lesion produced by HIFU using endo-tomography [37].

Macroscopically, tissue impedance depends on numerous parameters such as temperature, composition (membrane capacitance, quantity of intra- and extra-cellular fluids), structure etc. The spectral variation of tissue impedance shows frequency windows with decreasing impedance and regions with almost constant impedance. The windows where the impedance decreases with frequency are called dispersion regions. The dispersion regions are linked with defined frequency ranges and are

associated with defined relaxation mechanisms. The complicated behaviour of tissue impedance in the β -dispersion region is mainly caused by the semi-permeable cell membranes, acting as a complicated leaky capacitor. The current distribution between the intra and extra-cellular electrolytes are highly dependent on the frequency of the current injection. Thus, at low frequencies mainly the extra-cellular properties are measured, whereas the intra-cellular properties become increasingly important with frequency.

During pathological changes of the cell (oedema, ischemia, cancer cell proliferation) and during external influence (heating, pharmacological medication) the electrical parameters change. It is therefore possible to detect these changes as a variation of the complex admittivity. The impedance of a volume can be calculated from the impedivity, using equation 22 where the sample material is considered homogenous, $\rho = \text{constant}$.

$$Z = \frac{U}{I} = \frac{1}{I} \int E(r) \cdot dr = \frac{\rho}{I} \cdot \int J(r) \cdot dr = \frac{\rho}{I} \cdot \int \frac{J(r) \cdot A(r) \cdot dr}{A(r)} =$$

$$= \rho \cdot \int \frac{dr}{A(r)} = \rho \cdot K$$

equation 22)

Z is the impedance (Ω), U is the voltage (V), r is the length along the current path (m), A(r) is the current area at the iso-potential surfaces (m^2) and K is a geometry constant (1/m). Hence if the medium is considered homogenous in the measured region the admittivity or impedivity in the same region can be calculated by measuring the impedance for any probe with a known geometry constant. The geometry constant can be found by measuring the impedance in a medium with known admittivity or impedivity.

3.3 MICROWAVES, TUMT

TUMT is a minimally invasive method for treatment of benign prostatic hyperplasia, BPH. Briefly, TUMT causes coagulation necrosis in the prostate by absorption of microwave energy. Microwave applicators are of comparable size as the wavelength, due to the much higher operating frequency compared to RFA equipment. The operating frequency of our TUMT microwave generator is 915 MHz, resulting in wavelengths of 44 mm and 139 mm in muscle and fat respectively [24]. This device has a special permit to work in this frequency range, which is used for mobile phone communication. The frequency reserved for microwave equipment such as microwave ovens is 2450 MHz. However, the attenuation in the transmission line for these frequencies is too high. The wave length is comparable to the target and it is meaningful to apply wave theory including standing waves and reflection phenomena etc. The energy is transferred to the tissue mostly by capacitive coupling (field heating) or radiation.

All TUMT studies in this thesis were performed on the ECP-system, Comair AB, Sweden. The ECP was developed at Karolinska Hospital during the 1990's. Before applying power to the applicator, a treatment catheter is inserted in the urethra and a sensor probe is inserted in the rectum, figure 4. The urethral catheter contains the microwave applicator, cooling lumina, inflation lumina and an optical fibre for temperature measurements without any electromagnetic interference. The half wavelength applicator is thought to mainly work through capacitive coupling rather than radiation. The rectal probe contains three optical fibre lumina. In order to locate the applicator at the desired anatomical level in the urethra, the catheter is equipped with an inflatable balloon. The rectal probe contains three optical fibre lumina. In order to locate the applicator at the desired anatomical level in the urethra, the catheter is equipped with an inflatable balloon.

The ECP-system records most treatment parameters every second. The mean value of the temperatures is fed back to the regulator to control temperature levels. The treatment reverts to stand by mode if the temperature in the urethra or in the rectum reach pre-set alarm values. Under normal conditions the feed-back loop prevents this. Automatic compensation is made for temperature deviation incurred by the closeness to the cooling lumina. During treatment, the operator can choose a urethral temperature set value of up to 46 °C. During normal treatments when the system is stationary or near stationary, the actual-values are close to the set-values. The net power needed to keep this situation might tend to increase or decrease. This is displayed as a calculated parameter "heating resistance", chapter 4. The reflected and transmitted power is also continuously monitored with a double inverted directional coupler to determine the net power transmitted to the applicator.

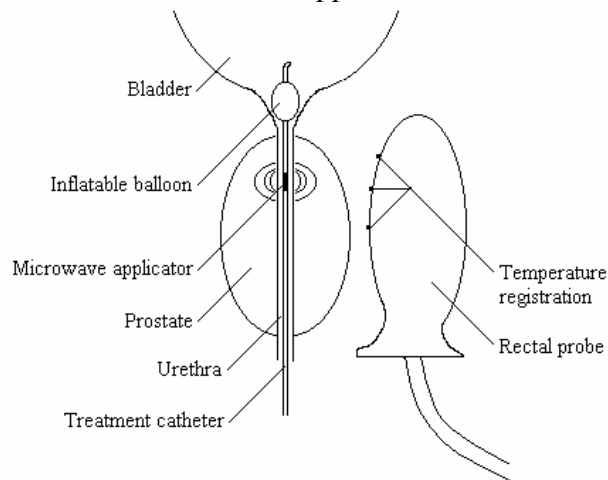


Figure 4. Probe and catheter setup in the patient for the used TUMT system, ECP, Comair AB, Sweden.

Without cooling of the catheter and the near nerve-rich tissue would reach very high temperatures even at relatively modest treatment power levels. Urethra related pain would therefore limit the treatment dose. The efficient cooling shifts the heat maximum deeper into the tissue, which enables higher output power.

The power density decreases rapidly with the distance from the applicator. The conductivity can be tenfold compared to RFA [38]. This is due to the changed absorption mechanism. The current is represented by alignment of permanent dipoles and/or dielectric polarisation (displacement of charges in the molecule) rather than movement of charged particles. Movement of magnetic dipoles is considered insignificant in tissues. The dipole absorption mechanisms are most pronounced in water resulting in selectivity due to the water content in the tissues at these high frequencies. Due to superposition and reflection, standing waves can occur in the tissue. This indicates a possibility to selectively choose a volume to be ablated. However, in practice it is difficult to predict reflection surfaces and the final standing wave pattern due to varying anatomy of the patients.

4 THERMOTHERAPY

Almost all of the discussed therapeutic methods in this thesis use temperature elevation to induce the beneficial therapeutic effects. Heating was recognised as a potential tumour therapy technique as early as 30 years before Roentgen discovered the x-rays. However, the technique has experienced relatively few clinical breakthroughs. This might be caused by the use of different heating protocols. There has been a limited use of a technique called hyperthermia [39-40]. Hyperthermia is characterised by relatively long exposure times at modest temperature elevation. These protocols often result in poor success rate without additional therapy such as radiation, giving the technique a surprisingly bad reputation. However, hyperthermia has been used with good results at a few centres over the world. Recently, a new heating protocol called thermotherapy has come into focus. In contrast to hyperthermia substantially higher temperatures and shorter exposure times are used. This also changes the mechanism of tumour cells damage.

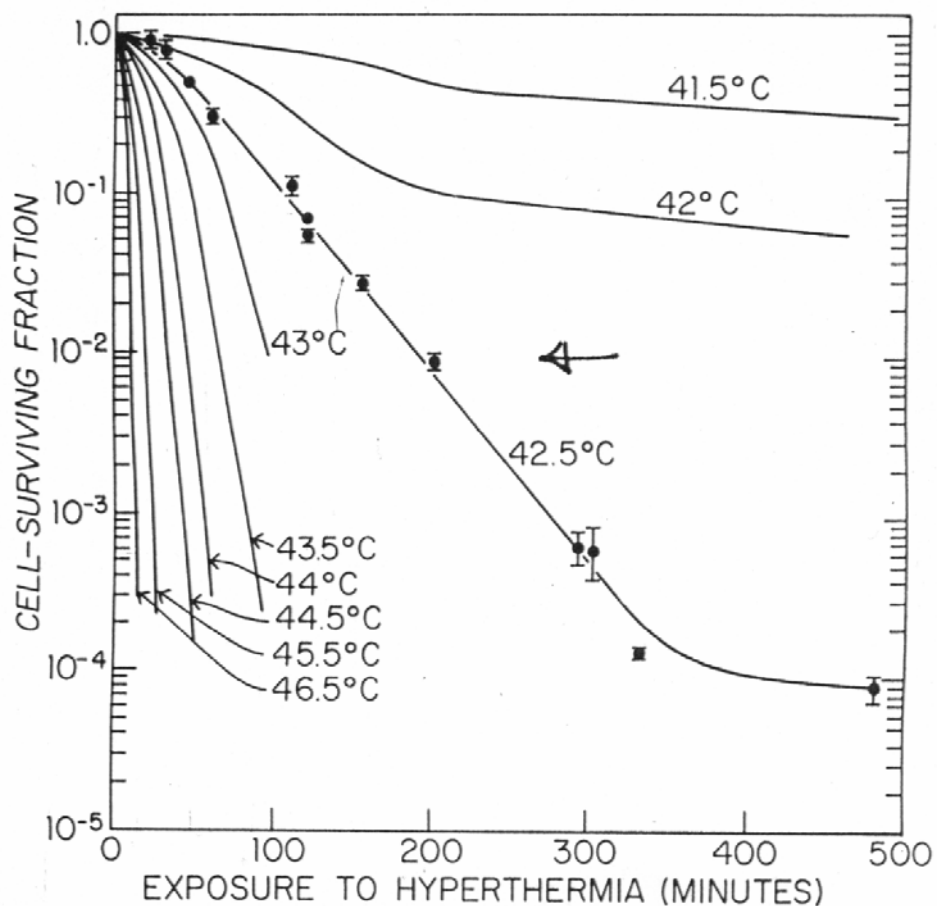


Figure 5. Survival curves for mammalian cells in culture (Chinese hamster CHO line) heated at different temperatures for varying lengths of time (redrawn from Dewey WC, Hopwood LE, Sapareto SA, Gerweck LE: Radiology 123:463-474, 1977).

The survival curves for mammalian cells exposed to temperatures under 43°C show a complicated behaviour, due to development of a resistance or tolerance that flattens the curve [41], figure 5. Thus at 41.5°C, approximately 70 percent of the cells are killed after 500 minutes. Over 43°C the resistance disappears and the survival curves steep considerably with increasing temperature. Under 60°C the cell damage is thought to originate from denaturation of proteins. The hyperthermia technique uses temperatures around 43°C, which makes it highly dependent on small temperature changes, requiring a very sophisticated temperature control.

Thermotherapy exposes the tissue to temperatures over 60 °C. At these temperatures the tissue coagulates because collagen is converted to glucose. The time frame of cell killing is considered almost instantaneous. When the tissue temperature reaches 100°C phase transformation of the intra- and extra-cellular liquid occurs. The glucose develops an adhesive effect after dehydration. Furthermore the cell membranes are likely to be disrupted by the increased pressure. The created vapour bubbles have a negative effect on both ultrasound and RF applications. In ultrasound applications the vaporised liquid shields the incoming ultrasound by reflection and consequently limits the target intensity. In RF applications the gas bubbles insulate the electrode electrically from the tissue, as discussed in chapter 3.1.

The temperature distribution and the thermal behaviour of tissues are governed by the bio-heat equation:

$$\rho \cdot c \cdot \frac{dT}{dt} = \nabla \cdot (k \nabla T) + \sigma \cdot |\nabla V|^2 - \rho_b C_b \omega (T - T_{amb}) + Q_m \quad \text{equation 23}$$

where ρ is the tissue density (kg/m³), c is the heat capacity (J/kg °C), k is the thermal conductivity (W/°C m), $\sigma \cdot |\nabla V|^2$ is the electrical absorption (W/m³), ρ_b is the density of blood (kg/m³), C_b is the heat capacity of blood (J/kg °C), ω is the blood perfusion (m³/s), T_{amb} is the ambient temperature (°C) and Q_m is the metabolic heat source (W/m³). This model states that the rate of temperature increase at a point is equal to heat transfer by thermal conduction, absorbed electromagnetic or acoustic power density, heat dissipation by blood perfusion and metabolic heating. Metabolic heating is often small compared to the other terms in the equation and is therefore often neglected.

The steady-state bio-heat equation for RFA in a homogenous material with a spherical electrode, equation 21 and 23, disregarding the perfusion and metabolic heat becomes:

$$\nabla \cdot (k \nabla T) = \frac{k}{r^2} \frac{d}{dr} \left(r^2 \frac{dT}{dr} \right) = - \frac{I^2}{\sigma} \left(\frac{1}{4\pi \cdot r^2} \right)^2 \quad \text{equation 24}$$

where r is the radius in the spherical coordinate system (m). The analytical solution to the coupled problem in equation 24 becomes:

$$T(r) = - \frac{I^2}{k \cdot \sigma \cdot 32 \cdot \pi^2 \cdot r^2} - \frac{C_1}{r} + C_2 \quad \text{equation 25}$$

We see that the electrical energy absorption add a quadratic component to the solution. The maximum temperature is always located at:

$$\frac{dT}{dr} = 0 \Rightarrow r_{\max} = -\frac{I^2}{k \cdot \sigma \cdot 32 \cdot \pi^2 \cdot C_1} \quad \text{equation 26)}$$

Thus, the location of the maximum is determined by the current, the thermal conductivity, the electrical conductivity and the boundary conditions. To obtain the same electrode surface area as our developed RFA electrode the spherical electrode radius should be 0.0028 m. At the electrode the temperature is set to 20°C, which is the same as the cooling media in the electrode. The outer boundary of the spherical tissue mass is also set to 20°C. With these boundary conditions the solution becomes:

$$T(r) = \frac{I^2}{k \cdot \sigma \cdot 32 \cdot \pi^2} \left(-\frac{1}{r^2} + 183.57 \frac{1}{r} - 1785.71 \right) + 20 \quad \text{equation 27)}$$

If C_1 is inserted into equation 26 the location of the temperature maximum will be located at $r_{\max}=0.00545$ (m), i.e. 2.65 mm from the electrode. Interestingly enough, r_{\max} is independent of the tissue properties. By choosing the input power so that the maximum temperature obtained is 100°C, $T(r_{\max})=100$, the temperature distribution can be calculated, figure 6. The radius of the lesion volume is predicted to be approximately 18.8 mm (50°C margin). The temperature distribution is independent of the tissue properties because all discrepancies in tissue parameters are compensated for by adjusting the current. Additionally, the resulting temperature distribution from treatments without electrode cooling and with a cooling media temperature of 0 °C were calculated by setting the thermal flux and the temperature at the electrode boundary to zero respectively. The 50°C margin increased 1 mm when the cooling media was decreased to 0°C. Hence, active cooling of the cooling medium seems to be a relatively expensive measure, with only a small increase in lesion volume. This was also concluded by Haemmerich and co-authors [42], with both FEM simulation and in-vitro lesioning. If the cooling media is omitted during the treatment the maximum temperature occurs at the electrode surface and the radius of the lesion volume (50°C margin) decreases to approximately 9 mm due to the decreased input power. The accepted power with cooling media is four times that of the accepted power with no cooling.

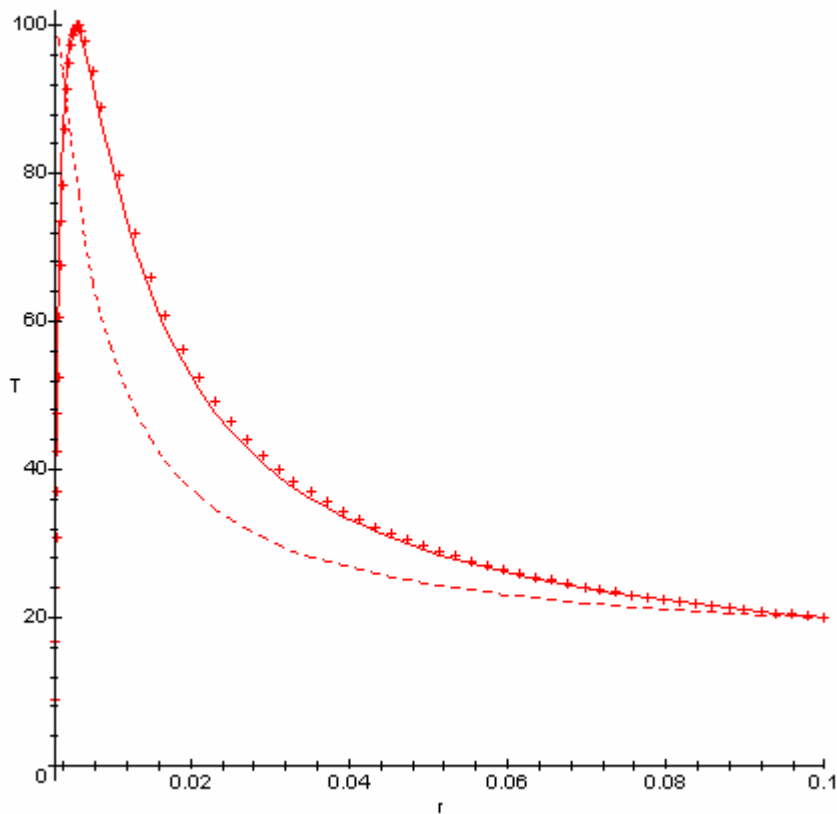


Figure 6. Shows the resulting temperature distribution from calculated steady state treatments using spherical current distribution. The solid and dotted curves correspond to treatments with a cooling media temperature of 20 °C and 0 °C respectively. Omitted electrode cooling is represented by line segments.

As tissue temperature increases more power is required to sustain the temperature due to increased thermal conduction and blood perfusion. It is known that blood vessels can increase their flow of up to 30 %. However, at sufficiently high temperatures the blood perfusion collapses and the net power to keep the temperature level tends to decrease. We suggest that the power to sustain a constant temperature, called “heating resistance”, should be plotted over time to serve as an indicator of micro perfusion (vessel) status in the treated volume. The heating resistance might be a powerful tool to measure the therapeutic result during thermotherapy.

5 FINITE ELEMENT ANALYSIS (FEM)

Except for extremely idealised models, solutions to the governing equations in chapter 3 and 4 can not be found analytically, requiring a numerical approach. FEM simulation is a powerful tool to transform differential equations over a volume to algebraic equations at points, called nodes [43-44]. These represent the solution to the governing equations and the boundary conditions in an average sense by piece-wise simple functions. The volume to be solved is divided into elements where for example the unknown electrical potential V is piecewise continuous. If sufficient continuity conditions are met, the solution converges to the exact solution as the number of elements increases. By an exact solution we mean the solution to the mathematical model which in turn often is an idealisation of reality. The nodes are often used as corners in the elements but they may also be on the edges and/or in the centre. The solution of a variable V is approximately represented within an element as:

$$V \approx \tilde{V} = \sum_{b=1}^n V_b \cdot N_b \quad \text{equation 28)}$$

where n is the number of nodes of the elements, V is the potential and V_b is the potential at the corresponding node b . The n shape functions N_b are polynomials, which values are unity at the corresponding node and zero at all other element nodes. The degree of the polynomials depends on the number of nodes in each element, and must be related to the defining equation. Increased polynomial degree improves the accuracy of the solution up to the actual degree of the governing equations, but requires more computational work.

In our studies a quadratic mesh consisting of quadratic (Lagrange) triangular elements were used for both the thermal and the electrical problem. The quadratic property indicates that the polynomial shape functions include quadratic terms, resulting in a quadratic dependence for the temperature or voltage and a linear dependence for the thermal flux or electric field within each element. For a triangular element these quadratic characteristics require six nodes, figure 7. The influence of each nodal value on the result within the element is also seen by examining the shape of the shape functions. If the quadratic elements are isoparametric the edges can be bent by transforming the nodal points with the same shape functions. This permits a more correct representation of bent boundaries in the model.

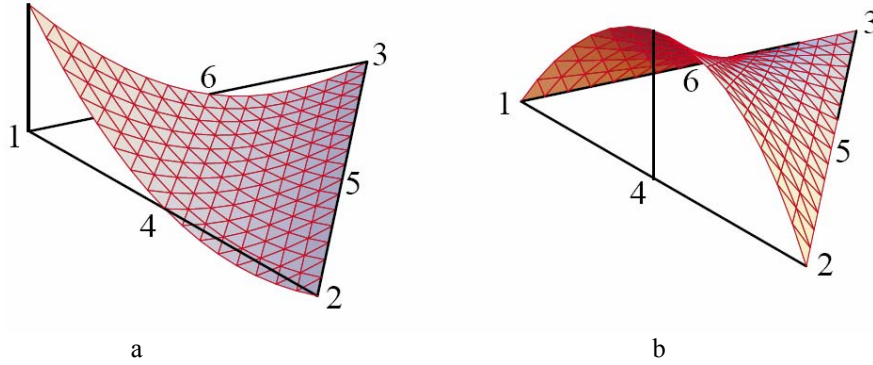


Figure 7. Shows the shape functions and the node placement for the used triangular quadratic Lagrange elements. a) represents the shape function for the three corner nodes and b) the edge nodes. The numbers indicate the placement of the nodes.

The amount by which the governing equations are not satisfied when approximating V is called the residual R

$$R = \bar{\nabla} \cdot \bar{\sigma} \cdot \bar{\nabla} \tilde{V} \quad \text{equation 29)}$$

Vector variables have both magnitude and direction and are presented with an over-bar. To find an optimal V we apply the method of weighted residuals to force the residual to equal zero in an average sense.

$$\int_{\Omega} w_a \cdot R \cdot d\Omega = 0, \quad a = 1, 2, \dots, n \quad \text{equation 30)}$$

where w_a is the one of the weight functions and Ω is the considered region. When using the Galerkin residual method, the weight functions w_a are chosen to be the shape functions N_a . Substituting equation 29 for 30, applying the chain rule and Gauss theorem provide:

$$\int_{\Omega} \bar{\nabla} N_a \cdot \bar{\sigma} \cdot \bar{\nabla} \tilde{V} d\Omega = \oint_{\Gamma} N_a \cdot [\bar{n} \cdot \bar{\sigma} \cdot \bar{\nabla} V] \cdot d\bar{\Gamma} \quad \text{equation 31)}$$

where Γ is the region boundary integral. Using the definition from equation 28, equation 31 becomes:

$$\sum_{b=1}^n \sum_{i,j=1}^3 \left[\int_{\Omega} \frac{\partial N_a}{\partial x_i} \sigma_{i,j} \frac{\partial N_b}{\partial x_j} d\Omega \right] \cdot V_b = \oint_{\Gamma} N_a \cdot J_n \cdot d\bar{\Gamma} \quad \text{equation 32)}$$

where J_n is the normal current out of the surface. The equation represents a set of n linear equations for the coefficients V_b . The matrix representation of equation 32 is:

$$[K] \cdot V = F$$

where

$$[K] = \int_{\Omega} [B]^T [\sigma] [B] d\Omega \quad n \times n \text{ stiffness matrix}$$

$$[B] = \begin{bmatrix} \frac{\partial N_a}{\partial x_i} \end{bmatrix} \quad 3 \times n \quad \text{equation 33)}$$

$[\sigma]$ = electrical conductivity matrix 3*3

$$[F] = \oint_{\Gamma} N_a J_n d\Gamma \quad n \times 1 \text{ force vector}$$

The key point of the finite element method is the local definition of shape functions, being defined only in one sub-region, and zero elsewhere. This significantly reduces the work needed to perform the above integrations, and also allows matrices, where large parts are zero, representing non-connected nodes in the region. The calculation of the K and F matrices involves numerical integration which also affects the accuracy of the results. The potential V_b at the nodes, approximately representing the true solution V is subsequently solved at the nodes with linear algebra. By using equation 28 the potential at every point inside the elements can then be obtained. To solve for example the bio-heat equation the same methodology is performed except the fact that the time derivative must somehow be estimated.

If the electrical conductivity is not dependent on the temperature the thermal and electrical equations can be solved independently of each other. Hence, the SAR value over the volume is obtained first by solving Laplace's equation, equation 20. Subsequently, the temperature can be found by solving the bio-heat equation, equation 23. However, when temperature dependent conductivity is used the equations must be solved simultaneously with increased computation as a consequence.

6 MICROWAVE ENERGY, EVALUATION AND IMPROVEMENT OF THE TUMT TECHNIQUE

Trans Urethral electro Resection of the Prostate (TUR-P) is the golden standard treatment for BPH. Since the middle of the 1980's new minimally invasive methods have been developed. TUMT is one of those relatively new techniques which are associated with significantly decreased morbidity and mortality rates [45]. Despite this advantage the technique is still controversial, probably due to the diverging clinical results. One suggested explanation to this discrepancy is the use of equipment with completely different heat patterns [46]. Earlier clinical studies have shown that the success rate is highly correlated with the power transmitted to the tissue [47]. However, numerous sham studies have shown a beneficial reduction of symptoms [48-52], supporting further use of TUMT. It is suggested that patients with mainly irritative symptoms experience a more beneficial reduction of symptoms. The therapeutic result originates from urethral denervation combined with volume reduction [53]. Due to the overall better reduction of symptoms associated with TUR-P the task at hand is to find the potential responders for the more lenient TUMT.

After a TUMT session in 1996, a transvesical enucleation of the prostate was performed one day after the treatment because of urinary retention and great difficulty in inserting a catheter [54]. The histological examination of the prostate showed a very marked and totally necrotic area in a circular shape having a diameter of approximately 20 mm, figure 8. The urethral mucosa was undamaged.

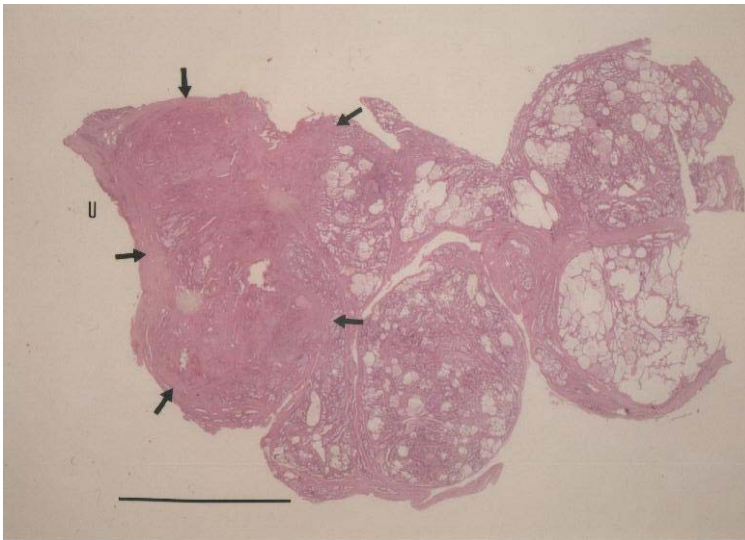


Figure 8. Whole mounted section of hyperplastic prostatic gland. Note the sharply delimited necrotic area (arrows) measuring approximately 10×25 mm. The urethral border is located at U. The bar represents 10 mm.

6.1 LONG-TERM CLINICAL OUTCOME OF TUMT USING THE ECP-SYSTEM

This TUMT evaluation was based on the ECP-system used at the Urology unit, Karolinska Hospital, Stockholm, Sweden. Between November 1991 and August 1999, TUMT was performed for BPH on 371 patients (45 - 94 years of age, mean age 76 years) during 427 sessions. At follow-up 69 were deceased. Since urodynamical and patient data in many cases was sparse, a questionnaire was designed and mailed to the treated patients. The questionnaire contained dedicated questions about BPH symptoms, the treatment, additional procedures etc. The patients were also asked to grade their BPH, at follow up compared to the situation before treatment.

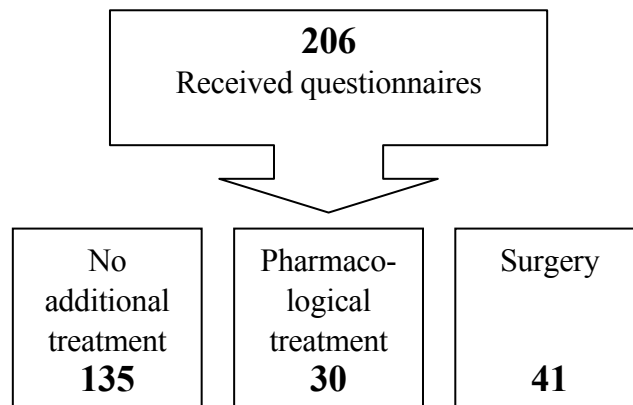


Figure 9. Additional treatment after the TUMT treatment.

One hundred and thirty five of the 206 patients who answered the questionnaire did not receive any additional BPH treatment, figure 9. Thirty underwent pharmacological treatment after TUMT in the form of *finasteride* or *α -receptor-blockers*. The remaining 41 patients received additional surgical treatment, mainly in the form of TUR-P. Four patients in the surgery group also received pharmacological treatment before surgery. Before TUMT 29 of the patients (14 %) had catheter a demeure (CAD). The mean micturition frequency during the night was 2.9 times, 58 % experienced urgency and 60 % low micturition flow.

The patients were asked to grade their improvement of BPH symptoms after TUMT. Seventy percent answered that the symptoms were reduced and 22 % judged that they had been fully cured. Initially all patients received 60 minutes of TUMT. However after a study by Bergman and Wiksell [55] it was concluded that 30 minutes was sufficiently beneficial and it henceforth became the standard treatment time. After the 30-minute-treatment, the IPSS and the QL decreased 37 % and 27 % respectively, for the no-additional treatment protocol. The 60-minute-treatment decreased the same IPSS and QL scores by 53 % and 38 % respectively. Hence, this study indicates that TUMT for 60 minutes provides better results than 30 minutes, which is the opposite of what was concluded in the earlier studies [52, 55]. Nonetheless, careful balancing between effective treatment and discomfort, where the patient is experiencing severe urge during treatment, is necessary. The beneficial reduction of symptoms was registered after one to a few weeks

subsequent to the treatment. In the patient group given pharmacological treatment in addition to TUMT, the IPSS and QL decreased 25 % and 28 % respectively after the 30-minute-treatment. In the surgery group, the decrease was 63 % and 50 % respectively (30-minute-treatment). Only a few patients experienced additional protocols after the 60-minute-treatment. Therefore, no significant data was obtained for these protocols.

In this study, we documented another very important quality of the TUMT treatment. Of the 29 patients who had CAD before TUMT, 8 (27 %) were permanently catheter free at follow-up, table 1. Six (21 %) patients still had CAD and 6 (21 %) used self-catheterisation (RIK). Nine (31 %) patients had experienced a supplementary TUR-P. Additionally, 4 patients (14 %) were catheter free at least 1 year after TUMT, but underwent TUR-P or re-received CAD. Consequently 12 (41 %) patients became temporary or permanently catheter free after the TUMT treatment.

Before TUMT	One year after TUMT				At follow-up			
CAD	CAD	RIK	TUR-P	Catheter free	CAD	RIK	TUR-P	Catheter free
29	4	6	7	12	6	6	9	8

Table 1. Description of catheter users before TUMT, one year after TUMT and at follow-up.

At follow-up 96 patients had not answered the questionnaire and 69 were diseased. One hundred and sixty-five TUMT-treated men were thus not followed-up. By phoning or reviewing case records, some data was available for 130 of these patients. Thirty-eight of these patients had CAD before TUMT. Ten of these 38 became permanently catheter free after TUMT. The outcome of 8 is unknown, 7 underwent TUR-P and 13 still had a catheter at follow-up. Hence, overall 18 of the 59 catheter patients (31%) with known outcome became permanently catheter free after the treatment.

Maximum micturition flow (Q_{max}) was available for 29 patients before and 1, 3 and 6 months after the treatment. One month after the treatment, Q_{max} had increased 21 %. At 3 and 6 months after the treatment, the increase was 14 % and 11 % respectively. This is surprisingly low compared to previous studies done on this equipment [52, 56]. The difference might be explained by our high baseline flow, which was not representative for our patient group (>10 ml/s is considered almost healthy). The behaviour over time, however, agrees with other studies [57], which include a rapid increase shortly after the treatment, followed by a slowly decreasing Q_{max} .

To improve the success-rate of the treatment several studies have been made to find baseline clinical parameters which can predict treatment outcome. However, no consistent results are reported. In this study we defined potential responders as patients with $Q_{max} > 10$ ml/s. In this patient group, 19 % considered themselves fully cured. In the group with $Q_{max} < 10$ ml/s, 11.8 % considered themselves fully cured after the treatment. If the limit is changed to 14 ml/s, 23.5 % of the predicted responders and 13.6 % of the

predicted failures considered themselves fully cured. Hence, in the responding groups almost twice as many consider themselves fully cured than in the failure groups. This suggests that patients with low flow obstruction before TUMT experience more beneficial reduction of symptoms.

Patients surgically treated with TUR-P, when TUMT proved unsuccessful, reduced their IPSS score more than other categories. TUMT has presumably failed because of the inclusion of non-suitable patients, for example with severe flow obstruction. TUMT has documented poor success-rate for these patients. TUR-P on the other hand, gives good relief from obstruction. We should also bear in mind that many patients in this study were chosen for TUMT because of their poor medical condition. Before the TUMT treatment 36 (17 %) patients had heart problems, 6 (3 %) had cancer in the urinary bladder or the prostate and 10 (5 %) had thrombi-embolic related diseases.

6.2 AUTOMATIC DETECTION OF CATHETER DISLOCATION

TUMT is associated with a very low risk. However, when accidents do occur it is often due to dislocation of the catheter, which might be caused by a ruptured balloon in combination with poor supervision. We have observed that bladder stone situations might mean a higher risk of balloon rupture. If the catheter is dislocated, dangerous heating of tissues other than the prostate might result, for instance the penis root. Dislocation of the rectal probe on the other hand might increase the power during rectally regulated periods. Hence, the rectal temperature will not be safely limited, resulting in the risk of rectal tissue damage. These serious complication risks might be prevented if an automatic detection of dislocations could be incorporated.

Our hypothesis was that there existed a correlation between transmitted power and monitored temperatures in the rectum. This correlation quality might also have a typical time delay due to the heat transport distances. If the correlation quality R is continuously measured at different delay times τ , both the value and the location of the maximum might change if relocation occurs. However, a too high false alarm frequency cannot be tolerated, which in turn puts demands on the signal to noise ratio for the involved signals. In some modes the output microwave power is almost constant during long periods, which might mean that the signal to noise ratio is too low. The basic function used to measure cross-correlation is:

$$R_{XY}(\tau) = \lim_{T \rightarrow \infty} \frac{1}{T} \int_0^T x(t)y(t + \tau)dt \quad \text{equation 34)}$$

This function will return a qualitative indication of the signal-resemblance between x and y dislocated τ seconds. In real life T must be finite and an approximation is therefore needed. T must be set to a value that provides a sufficient signal to noise ratio and at the same time terminates the treatment a few seconds after the catheter is dislocated. Therefore, a trade-off between fast response and sufficient signal to noise ratio is necessary. Actual data received from the ECP equipment is time discrete 8-bit samples. The discrete version of equation 34 becomes:

$$\hat{R}_{XY}[\tau] = \frac{1}{N} \sum_{j=1}^N P[j] \cdot T[j + \tau] \quad \text{equation 35)}$$

where P is the power (W) and T is the temperature (°C). During fifteen in-vivo sessions the ECP software was temporarily changed to include three additional file recording sequences, where the rectal temperature and output power data was saved each second in special files. This enabled us to develop a software environment where we could simulate the treatment and display the cross-correlation function. It further made it possible to manipulate parameters and data to optimise the program. Before calculating the cross correlation, the data was subtracted with a value equal to the mean of X previous samples, equation 36.

$$\hat{x}_i = x_i - \frac{1}{X} \sum_{i-X}^{i-1} x_i \quad \text{equation 36)}$$

This will reduce the effects of the dc component and slow changes in the temperature and power curve. Initially, some model studies were carried out to document correlation. In one study the catheter and the rectal probe were placed 20 mm apart in 500 ml isotone saline-water solution and the urethral fibre was thermally uncoupled relative to the simulation water tank. Data acquisition from 60 minutes of treatment using this setup can be seen in figure 10a. Initially, the treatment was not actively regulated because the rectal temperature and the urethral temperature were below the proportional regulator band. Consequently, the output power was maximised to a set value of 80 W, figure 10b. After 8 minutes, 42.5 °C was reached and rectal proportional regulation was initiated figure 10c.

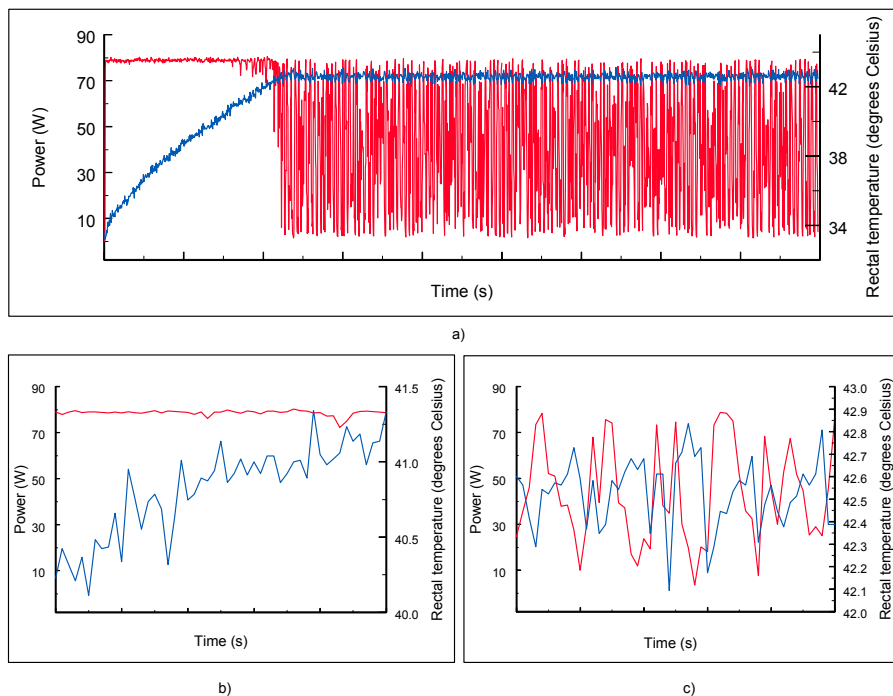


Figure 10. a) illustrates the whole treatment 0 - 1800 seconds. b) and c) show 50 seconds of non-regulated and rectally regulated periods respectively.

The non-regulated part of the curve showed no significant correlation. On the other hand a significant negative extreme point of the correlation existed for small negative τ values during the rectally regulated part. Furthermore, the correlation showed a damped oscillating behaviour with increasing τ . The negative correlation value and time delay at the extreme point originate from the rectal regulation of the ECP-equipment, i.e. the power is controlled by the rectal temperature, figure 10c. This is for obvious reasons not an evidence of correlation between power and temperature in the tissue, where both the correlation and the time delay should be positive, equation 35.

However, the periodicity in the correlation and the signals during the rectally regulated part suggest that such correlation exists, since no periodicity exists during the non-regulated part when the power is constant, figure 10. The existing correlation might originate from circulation of the medium near the catheter and thus show periodical fluctuations in the temperature not present in an in-vivo situation. Further, when the treatment is urethrally regulated, which most of the treatments are, the variation in power over time is much smaller. Moreover, the level of rapid variation in both the non-regulated and the rectal regulated part of the rectal temperature has the same amplitude, figure 10b-c. Conclusively, it seems hard to obtain a correlation in the in-vivo situation, especially during the urethrally regulated treatments.

Finally, fifteen in-vivo treatments were performed with the changed software at Karolinska Hospital. No cross correlation was found in either rectally or urethrally controlled treatments. If most of the absorbed energy in the rectum originates from thermal conduction rather than direct electromagnetic absorption the body will average any time variation.

6.3 CONCLUSION AND FUTURE WORK

The results from this study justify continued use of the ECP, which provides an effective, meaningful and lenient alternative to classical TUR-P. TUMT is performed on an outpatient basis and requires one skilled nurse operator. This makes the method extremely cost effective. The ability to perform the treatment on patients in bad general condition is extremely important considering the relatively aged patients. As a result, the patient foundation is often rather poor, for example 25 % of the patients had cancer or heart problems. It's important to remember that these facts negatively bias clinical evaluations.

The sixty-minute-treatment generates a more beneficial reduction of IPSS and QL-scores than the 30-minute-treatment. The IPSS score decreased 53% for the longer treatment. Combined TUR-P and TUMT treatment decreased the score by 63 %. The number of fully cured patients increased if $Q_{\max} > 10$ ml/s before the treatment. This indicates that patients with relatively moderate flow obstruction and mainly irritative symptoms experience a more beneficial reduction of symptoms.

Patients with CAD are usually suggested for TUR-P in our department. But because of the poor general condition of some patients or at the patient's own request, TUMT was carried out. Several of the patients had been through heart surgery and could be kept under anticoagulant treatment throughout the TUMT-treatment. Nevertheless 41 % of the patients with CAD were still catheter free one year after the treatment. If we also include the 30 catheter patients with known history, followed-up by phone or case-records, 18/59 (31 %) became permanently catheter free. The possibility to remove the catheter significantly decreases the infection risk associated with catheter use and increases the quality of life. This catheter-removal effect has been investigated in relatively few reports and is an important finding that should be further explored on every TUMT system.

The study is limited due to the poor answering frequency. However, the larger number of patients and the longer follow up period compared to other studies justify investigation of the data. The patients that did not answer the questionnaire were in many cases not capable of a subjective judgement due to for example Alzheimer. The relatively aged patients make good subjective retrospective studies hard to perform. However, the catheter status was followed-up on 91 % of the patients, which is the most important finding in this study.

Furthermore, attempts to improve the safety of the treatment by detecting dislocations of the probes, using the cross correlation between the output power and the rectal temperature, were performed. Unfortunately, this does not seem to be feasible due to the suggested averaging effect of the thermal behaviour. Another simpler but probably more unreliable method could be to halt treatment when the temperatures or the input power show transient behaviour.

7 DEVELOPMENT OF RF-TECHNIQUES

7.1 RFA TREATMENT OF BREAST TUMOURS

At least one in ten women in the western world faces the prospect of developing breast cancer. The tendency in modern treatment of these tumours is towards less invasive local treatment. Today breast conserving surgery has become more common than mastectomy in many countries. The goal is to remove all of the cancer together with a sufficient margin of healthy tissue, to prevent local recurrence. Another objective in modern therapy is to minimise the alteration of the breast configuration. Recently other approaches than traditional surgery have been explored to satisfy these demands [58-59]. These techniques are minimally or non-invasive and include, cryosurgery, stereotactic excision, laser ablation, focused ultrasound and radio frequency ablation (RFA). Potential benefits with these techniques are reduced morbidity rates, reduced treatment duration, ability to perform therapy even when patients are in bad medical condition and to keep the procedure on an outpatient basis. Furthermore, many breast cancers are today detected at an early stage by mammography screening, increasing the effectiveness of the minimally and non-invasive techniques such as RFA. The cosmetic and oncologic results of these new methods are yet to be evaluated. The RFA technique is well tested for use in organs such as liver, prostate, bone, brain and kidney [28].

The objectives for this study were to develop a RFA system with internally cooled electrode needles and to perform in-vitro RF protocols on excised breasts with tumour. The developed equipment consists of a specially designed RF-generator with floating low impedance output (0-950 W, approximately 1.5 MHz) and a dedicated autoclavable lesion electrode with integrated temperature monitoring and water cooling system. The needle is composed of two cannula tubes with diameters sufficient to permit a predetermined flow. The external cannula is 2.1 mm in diameter and surface insulated except for 20 mm at the tip, figure 11. A teflon insulated constantan wire is laser welded to the outer cannula, not shown.

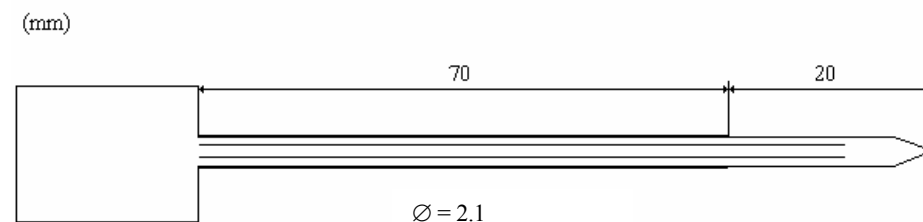


Figure 11. Shows the dimensions and the cooling media paths for the cooled RF electrode.

We have chosen thermocouples to measure temperature because they can be easily miniaturised to ensure minimal cooling water obstruction in the thin design plus an adequate short time constant. The very low signal level obtained from the thermocouples ($53 \mu\text{V}/^\circ\text{C}$) suffers interference from the applied RF-power field, approximately $100 \text{ V}_{\text{rms}}$. This demands that the low-pass filtering before amplification has very high damping. The RF signal

was damped approx. 70 dB with a tuned low-pass filter. The RF-power feeding and low-level feed-back circuits must further be cardiac floating (CF) according to EN 60 601-1 international specifications (patient leakage current, PLC, less than or equal to 10 μ A, frequency weighted). The whole temperature circuit has been built using a Faraday cage design. The temperature measurements are also compensated for cold junction temperature variations by a feed-back method.

In order to attain the SAR distribution surrounding the needle, the potential difference between a specially designed measuring probe and the needle $V(x)$ was measured at different distances x , figure 12. Protocols were carried out in saline solution and in muscle tissue. An aluminium cauldron, radius 160 mm and height 265 mm, served as the indifferent electrode.

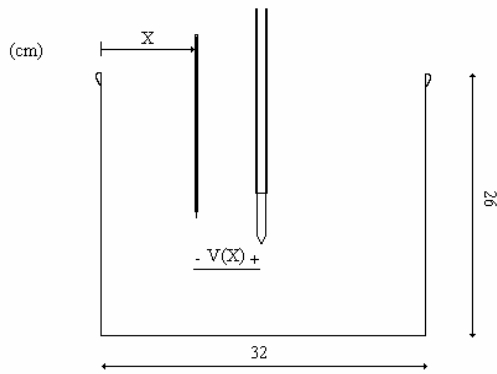


Figure 12. Shows the experimental set-up to measure the SAR around the RF-electrode

The power distributed inside the iso-potential surface with the radius $16-x$ is $V(x) \times I_{in}$, where I_{in} is the total current from the generator. The power $P(x)$ divided by the total power distributed in the buffer $P(0)$ provides us with a measurement of how much of the power that is absorbed inside the iso-potential surface compared to the total absorbed energy in the cauldron, equation 37.

$$\frac{P(x)}{P(0)} = \frac{V(x) \cdot I_{in}}{V(0) \cdot I_{in}} = \frac{V(x)}{V(0)} \quad \text{equation 37}$$

The measured quota in equation 37 is plotted with respect to x in figure 13.

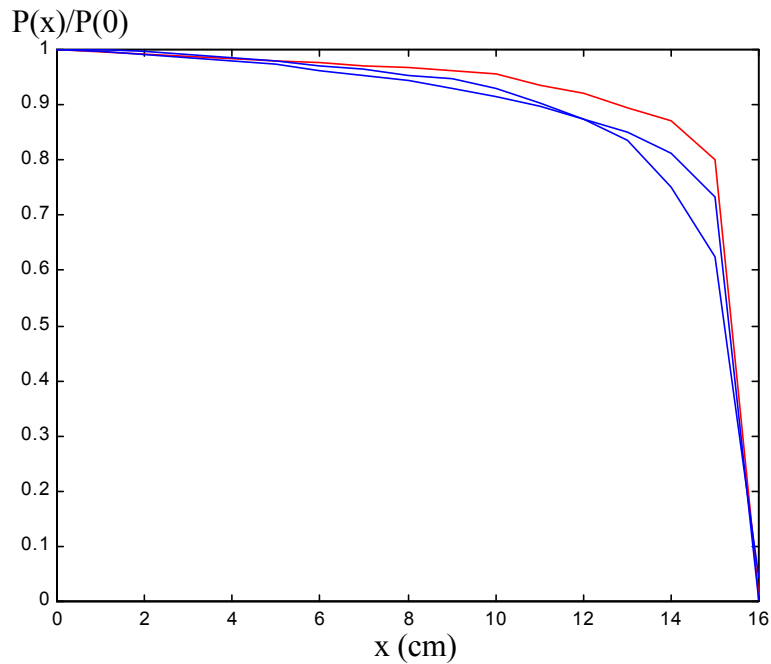


Figure 13. Shows how much of the power that is absorbed inside an iso-potential surface with radius x -16 compared to the total absorbed energy in the cauldron for saline solution and muscle tissue. The two plots showing the lowest absorption near the electrode are measured in 0.9 % saline solution. The highest absorption was obtained in muscle tissue.

Eighty and eighty-seven percent of the total power is absorbed in a small volume with a radius of 20 mm in saline solution and muscle tissue respectively. Hence, almost all of the energy is absorbed in the near region of the needle. This is a geometrical effect, discussed in chapter 3.1 equation 21, which to a great extent determines the lesion volume.

Our group have an accepted ethical approval to perform RFA treatments on excised human breast material with tumour. After obtaining informed consent four patients underwent modified radical mastectomy because of breast cancer, verified by preoperative fine needle biopsy [60]. After the surgical procedure the specimen was sent to the pathologist. From the fresh breast specimen a slice of the tumour was removed to ensure material for diagnostic purpose of the viable tumour and to establish resection margins. Subsequently, the tumours were RF-ablated. The maximum tissue temperature was maintained at approximately 100 °C during 15 min. It is difficult to measure the true maximum temperature due to the circulating cooling media, i.e. the true maximum point is located in the tissue. We have developed an algorithm that compensates for the deviation between the maximum temperature and the measured value at the tip. The electrical impedance was measured to ensure that no phase transformation of the tissue occurred. The temperature and the flow of the cooling media were set to 20 °C and 12 ml/s, respectively. An electrode current of 0.35 – 0.71 A_{rms} was applied during the procedure. The impedance decreased up to 50 % during the treatment.

All treated tumours were 30 mm or more. Three were ductal carcinomas and one lobular carcinoma. The cellular changes were evident in the tumour structures as well as in the surrounding connective tissue but were also seen in tumour strands extending far from the main tumour. The adjacent fat

tissue showed only a very slight degeneration, but was otherwise surprisingly unaffected. The ductal carcinomas showed no areas with viable tumour. In contrast the lobular carcinoma with its irregular outline and diffuse growth showed tumour cells with preserved viable appearance in the surrounding fat at a short distance from the coagulated area around the electrode canal, suggesting an insulating effect of the fat tissue. Interestingly, the heat pattern appears to be drawn to the tumour in the tumour strands extending from the core tumour. The origin of this effect might be the dissimilar physical parameters in the tumour and in the fatty tissue. Adipose tissue has substantially different electrical properties compared to the tumour [61].

A theoretical study was carried out to study if the discrepancy in electrical or thermal parameters could cause the discussed tumour targeting effect. FEM analysis was used to solve the governing electrical and thermal differential equations, chapter 5. To correctly mimic the SAR-situation during RF ablation a 3-D model must be used, i.e., the iso-potential surface must increase with the squared distance from the needle. This is for obvious reasons not the case in 2-D or 1-D Cartesian models. However, if the situation demonstrates rotational symmetry a two dimensional axially symmetric model can be used instead, to decrease calculation time and the needed computer resources. In our case non-linear solving and the use of different tissues made rotational symmetry essential.

Description of cases		Tumour properties (mm)		Const/Temp dep σ	Time dep/ Steady state
		Thickness	Length		
1	Homogenous fat model	-	-	C	S
2	Homogenous fat model	-	-	T	S
3	Homogenous tumour model	-	-	C	S
4	Homogenous tumour model	-	-	T	S
5	Fat with an incorporated cigar shaped tumour	4.7	52	C	S
6	Fat with an incorporated cigar shaped tumour	4.7	52	T	S
7	Fat with an incorporated cigar shaped tumour	4.7	104	T	S
8	Fat with an incorporated cigar shaped tumour	4.7	26	T	S
9	Fat with an incorporated cigar shaped tumour	9.4	52	T	S
10	Fat with an incorporated cigar shaped tumour	2.35	52	T	S
11	Homogenous fat model	-	-	T	T
12	Fat with an incorporated cigar shaped tumour	4.7	52	T	T

Table 2. Shows the properties of the 12 cases in this study.

The FEM model consisted of an electrode with the same dimensions as in figure 11, which was placed in a spherical tissue mass, with a radius of 0.1 m. Initially, models with a homogenous tissue mass consisting of tumour or fat were modelled, table 2. Subsequently, the fat tissue model was modified to also include tumour. The tumour was cigar shaped with varying length and thickness, figure 14. Both constant and temperature dependent conductivity was used to assess if this had any effect on the lesion volume. All the above models were computed using steady state solving. To better mimic a real treatment, the power should be continuously controlled to hold

the maximum temperature at 100 °C during the whole treatment. Further, to prevent the effects of thermal conduction to be overestimated, the duration of the treatment should be approximately 15 min. Hence, to attain the same time frame as in the in-vitro experiment and include controlling, we performed two time dependent controlled treatments, table 2. One simulation was carried out on homogenous fat as in the steady state case 2. Subsequently, a cigar shaped tumour was placed in the fat model with the same size as in steady state case 6.

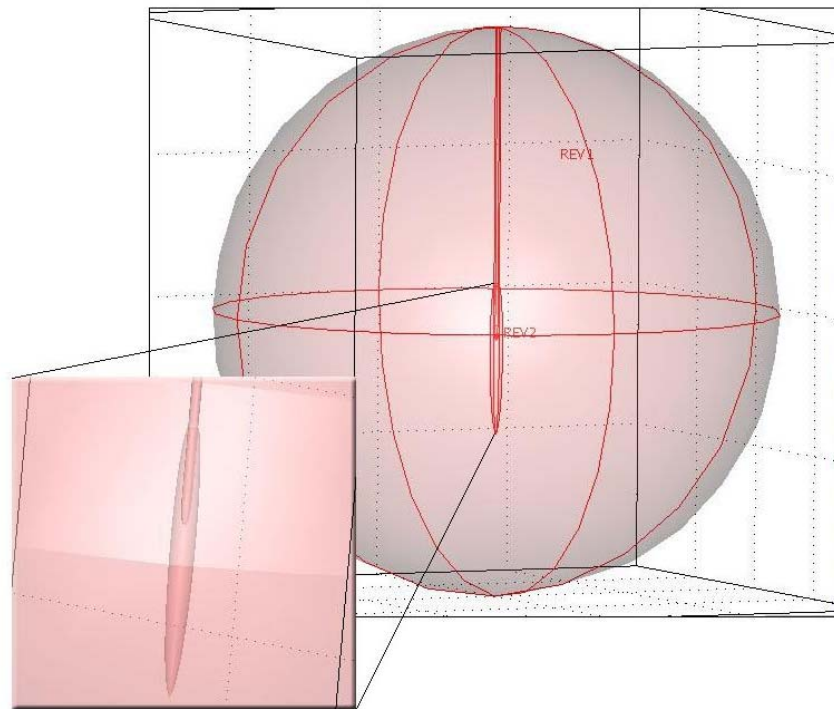


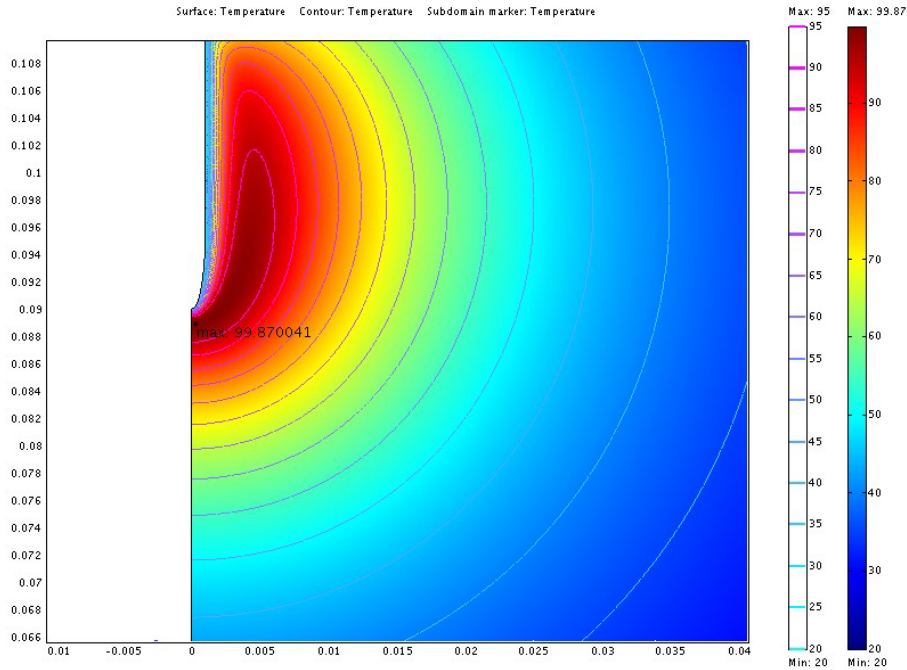
Figure14. The spherical model volume ($d = 200$ mm) with the electrode and the cancerous tissue. The tumour dimensions in this situation are $52\text{mm} \times 4.7\text{mm}$.

The cooling of the needle was incorporated in the model by setting the boundary to the cooling media temperature. The outer spherical boundary of the tissue mass was electrically grounded and set to maintain the initial tissue temperature during the whole treatment. In case 1-10 the voltage of the active part of the needle was adjusted to a constant value, due to the steady state solving, which resulted in a final maximum temperature of 100°C. In case 11 and 12 the input voltage was continuously changed to keep the maximum temperature at 100°C during the whole treatment. Lesion size was determined using the 50°C margin. Even though the lesion volume is dependent on both temperature and time of elevated temperature, similar lesion dimensions have been obtained using both thermal dose and threshold temperature [62].

The 50 °C lesion margin moved approximately 1-2 mm further from the electrode when temperature dependent conductivity was used in the simulation. Thus, only temperature dependent electrical conductivity was used to document the effect of tumour spatial shape and the influence of time dependence. The resulting temperature distribution, using temperature

dependent conductivity, from simulations with only fat tissue (case 2) and fat with embedded cancer (case 6) are shown in figure 15.

a)



b)

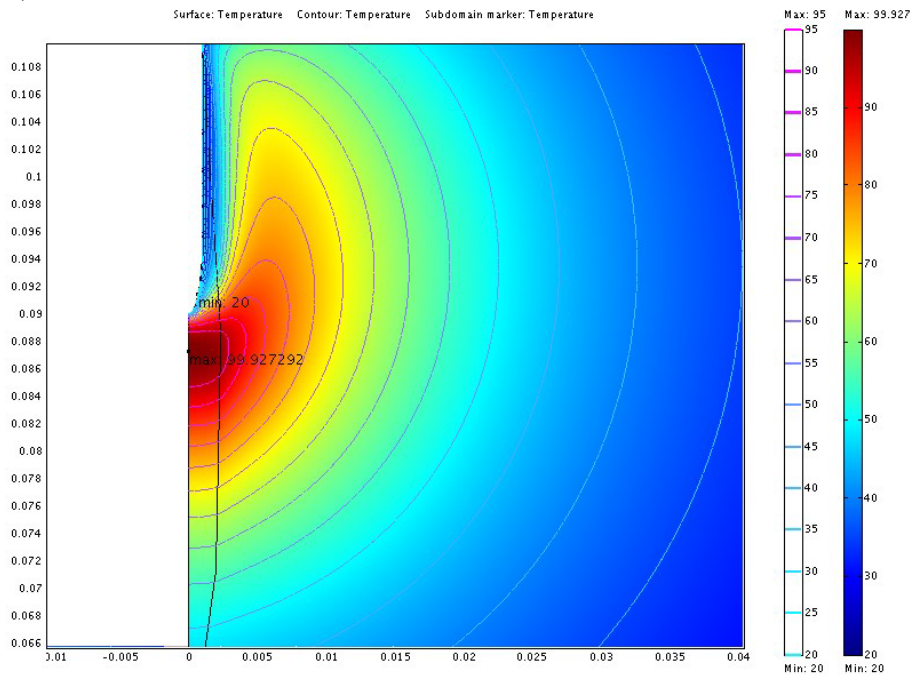


Figure 15. Temperature distribution from simulation with only fat tissue 15a (case 2) and from simulation with cancer embedded in fat 15b (case 6) using temperature dependent conductivity. The horizontal axis is denoted r and the vertical axis z . The coordinates are cylindrical and the symmetry axis is located at $r = 0$. The length scale of the axes is meter. Isothermal lines from 20 to 95 °C in steps of 5°C are also shown. The needle tip is located at $Z = 0.09$. The rough shape of the tumour is misleading because the Bezier curves are represented by a finite number of line segments.

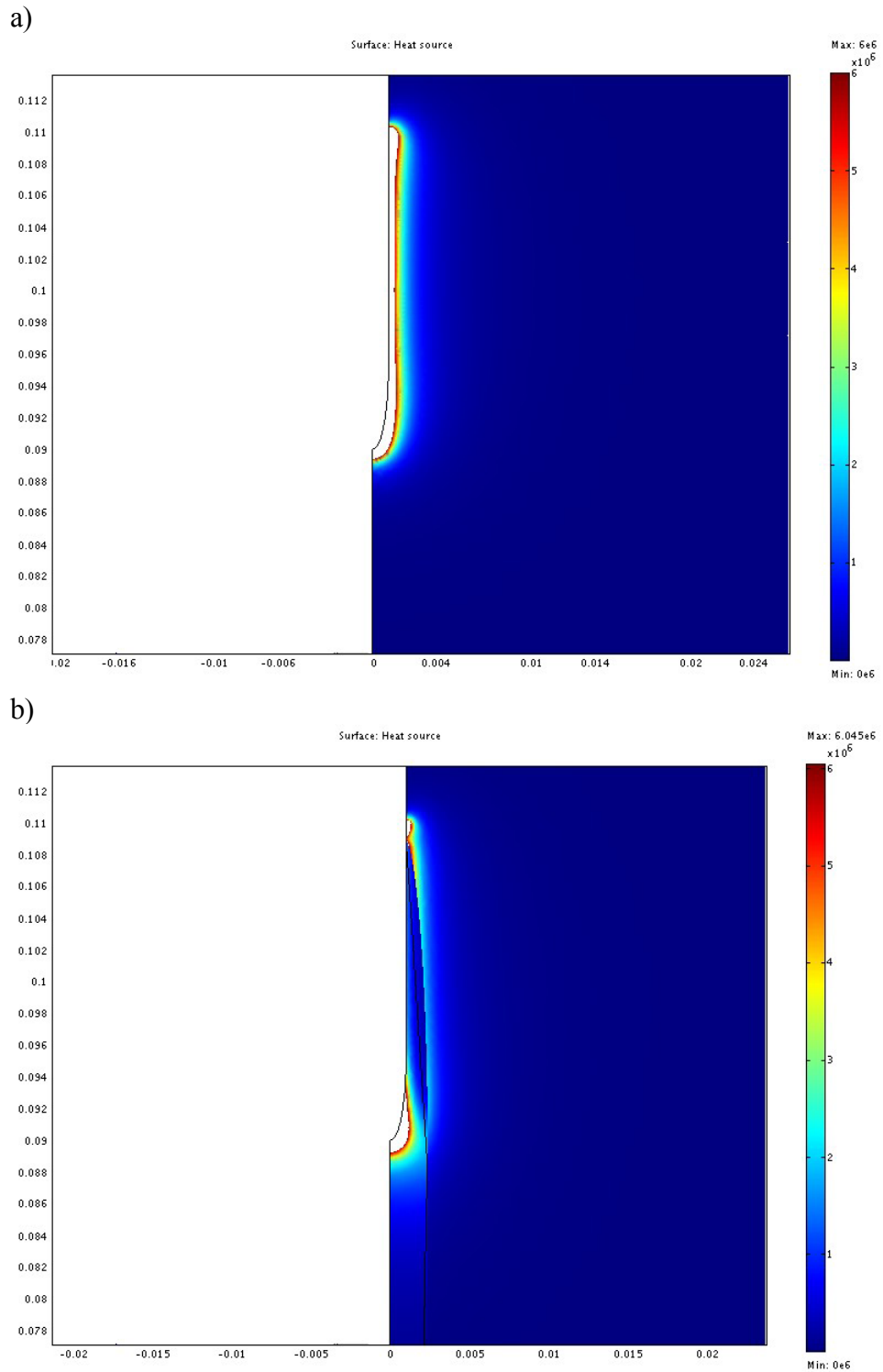


Figure 16. The distribution of absorbed power density for the same situation as in figure 15. 16a corresponds to case 2 and 16b to case 6.

In the homogenous fat model the maximum temperature is pushed away from the electrode by the cooling media in the electrode. Due to the non-uniform SAR distribution along the electrode shaft the maximum temperature occurs at the needle tip, figure 16a. The difference in temperature distribution between cases with and without tumour is primarily explained by the shift in electrical power density, figure 16. In the models with tumour, the power density in the tumour is higher than in the fat. The tumour increased the lesion (50 °C margin) by 4.7 mm along the tumour

length and decreased it by 1.5 mm perpendicular to the tumour. However, the relatively higher temperature in the tumour compared to the fat seems to decline with distance from the electrode. This is due to the geometrical effect of the power density, discussed in chapter 3.1. The temperature profile does not substantially change when altering the length of the tumour, figure 17. The width of the tumour on the other hand has a considerable effect on the temperature along the tumour. Both the lesion margin and the location of the temperature maximum were pushed from the electrode with increasing tumour width. Altering of the tumour length only changes the tumour in the region where the contribution to the total impedance is small. Thus, almost no effect on tumour length is detected.

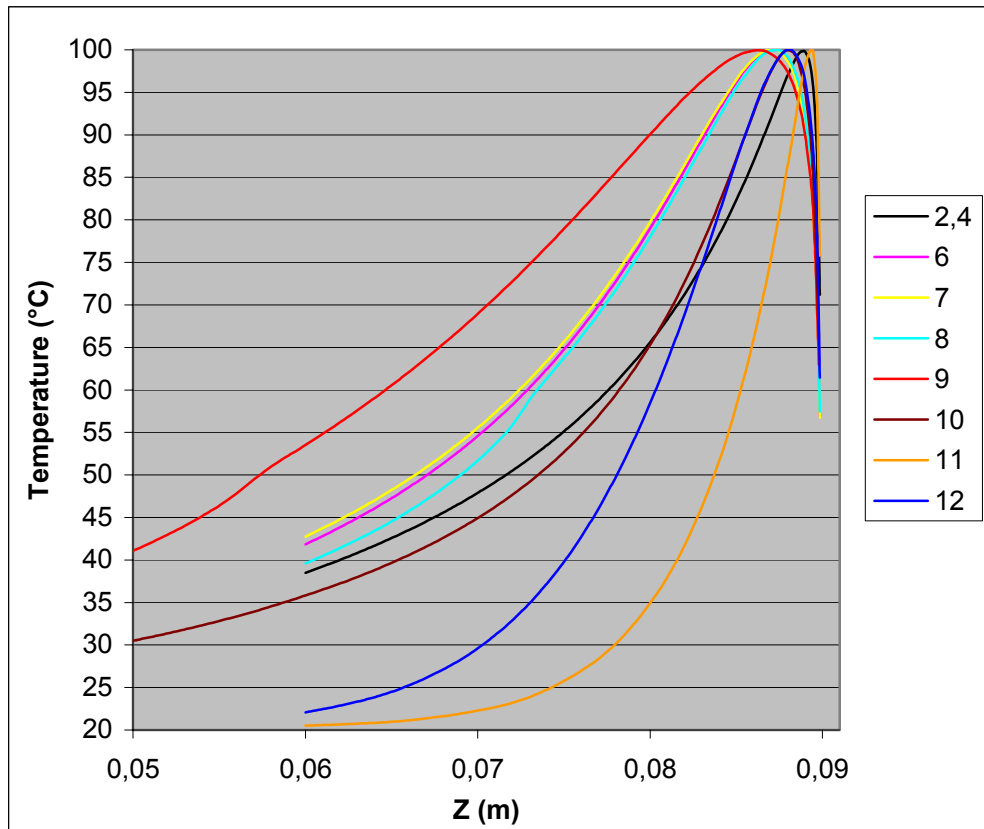


Figure 17. Temperature distribution along the symmetry axis $r=0$ for different tumour sizes compared to homogenous models 2 and 4. The two controlled time dependent simulations are also shown, case 11 and 12. All shown cases used temperature dependent conductivity. The needle tip is located at $Z = 0.09$.

During the major part of the treatment the increase in lesion volume is caused by thermal conduction in the distant regions. Hence, the electrical parameters are governing the heating process near the electrode during the initial phase whereas further away the thermal parameters become increasingly important during the last phase. The similarity in cases 2 and 4 is explained by the steady state solving and the temperature normalisation at 100°C , chapter 4. That is, all the time derivatives are zero and the voltage is set to obtain the same final maximum temperature and thus compensates for the difference in the thermal and electrical conductivity.

The controlled time dependent solutions in cases 11 and 12 create smaller lesions than their steady state counterpart, figure 17. The lesion volume decreased because of the shorter treatment time, i.e. less energy is transmitted by thermal conduction to heat the distant regions. However, the difference between tumour and non-tumour cases is larger during the controlled time dependent cases. During steady state simulation thermal conduction has progressed further and thus also smoothed out the temperature differences. Additionally, the difference in electrical parameters between fat and tumour is much greater than in the thermal parameters, which consequently increases the differences between tumour and non-tumour cases for smaller lesions where electrical parameters are more dominant.

7.2 PROVOCATION OF BLOOD CLOTS

In an ongoing project, we have used pulsed HIFU to dissolve thrombus formations in-vitro [6]. To document this effect in-vivo, thrombus obstructions must be induced in relevant vessels such as the coronary arteries. The aim of this study was to develop a fast and reliable provoking method in a laboratory animal model similar to humans. The animal vessels must therefore be of comparable size and match the flow conditions and pressure dynamic forces of the human vessels of interest.

We have developed a method to induce thrombi in the carotid and femoral arteries in a pig model using RF energy. Virtually all thrombus-provoking methods induce an endothelium damage to initiate the coagulation cascade and facilitate the adhesion between the vessel wall and the thrombus material [63-69]. Human coronary thrombi consist of both platelet rich and erythrocyte rich zones [70]. Authors have reported erythrocyte, fibrin and pallet rich thrombi independent of the techniques that were used to induce the endothelium damage [63-69]. The used techniques are associated with drawbacks such as low reproducibility, long procedure duration and the use of too small animal models to match the conditions of the human counterpart.

In our technique, RF energy at 140 kHz is used to generate the endothelium damage. The energy is applied to the body through a bi-polar catheter that is introduced in the vessel of interest, figure 18. After exposure to approximately 6 W during 30 seconds, the arteries were manually occluded for 15 minutes with ligatures.

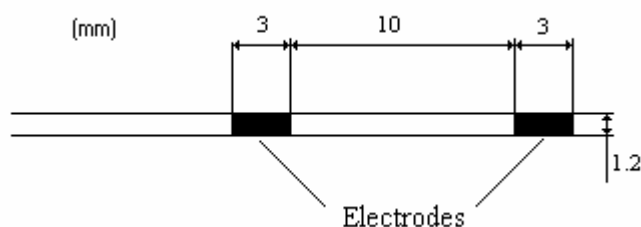


Figure 18. The tip of the used bipolar Cordis catheter.

Subsequently, the obstruction was removed and the blood flow was measured with a monodynamic ultrasound Doppler unit. The arteries were later removed and visually examined, figure 19. All 11 of our protocols resulted in a complete occlusion of the artery, i.e. no Doppler velocity reading and a visual thrombus mass filled the whole lumen.



Figure 19. Thrombus formation resulting from an artery exposed to 6 W. 30 seconds of exposure followed by obstruction of blood flow for 15 minutes resulted in totally occlusive thrombus in 11 of 11 arteries.

Using a static dose may cause severe or insufficient damage to the vessel wall because of for example varying blood flow in the in-vivo situation. Additional in-vivo protocols in muscle and artery were made to investigate the electrical properties and the temperature characteristics during exposure. During the initial phase of all tissue exposure protocols the electrical impedance decreased as the temperature increased over time. This is simply an effect of the temperature dependent conductivity. Suddenly the impedance abruptly increased, coinciding with a decrease in the temperature curve accompanied by a cracking sound, figure 20a-b. This avalanche phenomenon is further explained in chapter 3.1. The time interval from the application of power to the impedance increase varied for different tissue protocols. For protocols with less or no tissue blood perfusion the increase occurred earlier than protocol with blood perfusion.

The sound associated with the breakpoint between the slow decrease and the sudden increase was further studied. In order to analyse the audible sound components of the signal we developed an amplitude demodulator, mainly consisting of a screened unit with diodes and low pass filter. The demodulated signal was fed to a low frequency power amplifier connected to a loudspeaker and in some cases also to a digital signal analyser. During the initial heating phase the amplitude modulation was low and no sound was heard from the speaker. During the final non-linear phase, associated with the impedance increase, the amplitude modulation increased significantly and contained noise-like components of up to approximately 8 kHz. A hissing sound could be heard from the speaker.

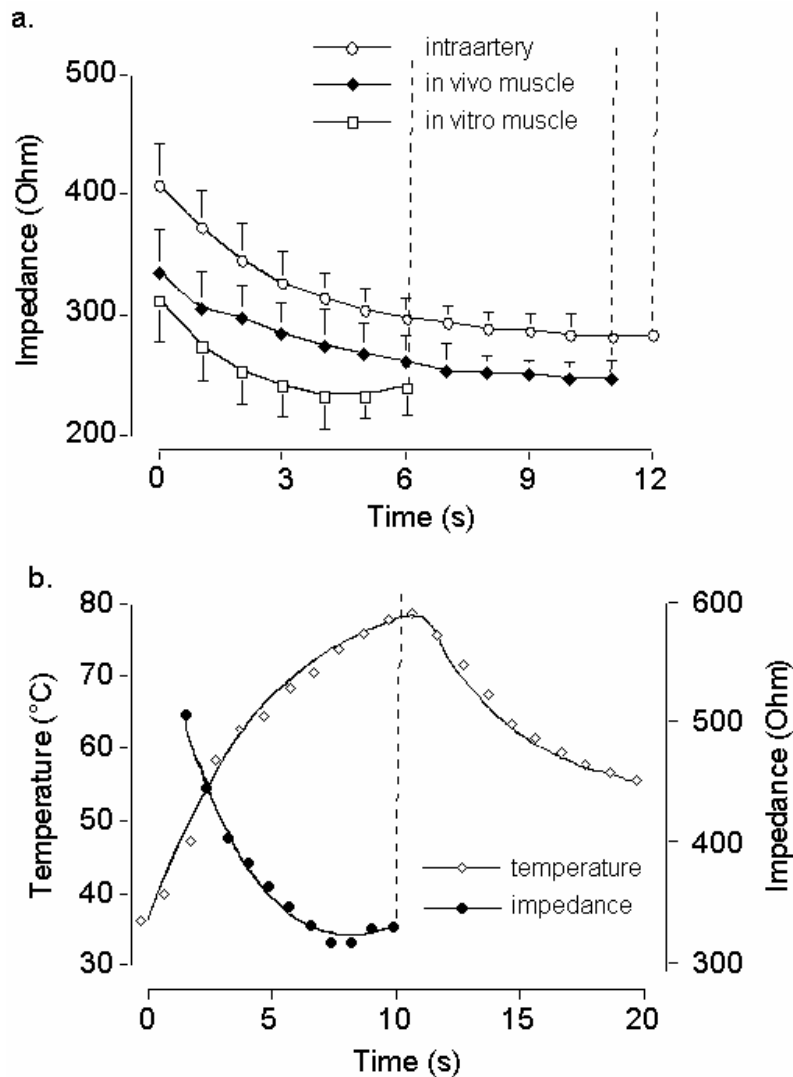


Figure 20. a) average impedance curves for all tissue protocols. Initially the impedance has a moderate negative slope but is suddenly increased in all protocols. b) temperature and impedance curves from an intra-arterial protocol showing that the abrupt impedance increase and the maximum temperature coincide in time.

7.3 CONCLUSION AND FUTURE WORK

We have developed a cooled monopolar RFA-system for treatment of breast tumours. Conclusively, ductal carcinomas seem to be well suited for thermotherapy with RF-energy, partly due to the thermal targeting effect of the tumour. A FEM study was performed to assess if the differences in physical parameters could invoke this effect. The presented tumour shapes in the FEM model do not claim to be a perfect representation of the real life situation. A better model would include a core tumour from which thin tumour strands extend. However, this is impossible to achieve with rotational symmetry, and with present limitations in computational resources. Additionally, such model would have too many variables to easily assess any conclusions.

The tumour targeting effect observed in the in-vitro studies was more pronounced than in the FEM models, especially in the long tumour strands extending from the core tumour, indicating that additional effects might be involved. Perhaps the membranes between the tumour and the surrounding tissue could have an additional electrical or thermal insulating effect. Thermally insulated membranes would increase the targeting effect further away from the electrode where the thermal parameters dominate. Subsequent studies should study what effect such membranes could have on the temperature distribution.

Our research group have an accepted ethical approval to perform in-vivo RF-treatment on 5 patients in the same anaesthesia-session as standard full mastectomy is performed. The results will subsequently be assessed by examining the removed specimen. If the tumours are completely killed by the RF-energy the next step is to file a new ethical application to use RFA as the only treatment method. The demarcation zone in the in-vivo situation will probably become more defined due to the collapse of the blood perfusion.

We have also used RF-energy to develop an efficient method to provoke arterial thrombosis. The study was performed in a relevant porcine model which is suitable for thrombus research taking size and the similarity of the clotting properties with humans into account [71-74]. The behaviour of the temperature and the electrical properties, along with their influence on the heating process will serve as tools to monitor and refine the control of the procedure. We suggest that the impedance minimum or the onset of modulation on the RF signal will serve as potential indicators to reduce the power allowing more standardised damage to the endothelium. The time for the whole obstruction procedure is less than 20 minutes. This method will later be used to document re-perfusion with our non-invasive ultrasound technique in the in-vivo situation.

8 ACOUSTIC TECHNIQUES

Acoustic energy or ultrasound is extensively used in medical applications in modern health care. Most often, the image producing diagnostic application comes in mind when ultrasound is mentioned. However, acoustic energy is also widely used in therapeutic applications such as ultrasound aspiration, ESWL, muscle therapy and cell lysis. High intensity ultrasound applications have been studied since the beginning of the sixties without any major breakthrough, mainly due to the unpredictable and inhomogeneous target alteration. Our research group have primarily focused on two applications, dissolving of blood clots and tumour ablation, using both heat and mechanical phenomena.

8.1 HIFU TREATMENT OF TUMOURS

It is our intention to evaluate the possibility of using high-energy focused ultrasound as a non-invasive modality to generate lesions in small breast tumours. Both the thermal effects and the micro-mechanical effects from cavitation bubbles will be investigated. HIFU therapy is associated with serious drawbacks preventing it from reaching clinical use. The focus volume is often limited in order to reach therapeutic intensities in the focus without damaging surrounding tissue. The focus is consequently swept over the target region making it difficult to create homogenous lesions. This also increases the treatment time substantially. Moreover, the treated regions influence the following ultrasound sweeps by for example shielding. This effect along with other non-linearities makes it extremely difficult to predict the target alteration. In an ongoing collaborative study by Jernberg, Hedlöf, Heiden, Ekstrand, Wiksell, Brahme, Lewensohn and Edgren [75] the non-thermal effects of ultrasound alone and in combination with γ radiation on human lung carcinoma cells are studied. The preliminary results show that non-thermal HIFU alone is capable of inducing immediate cell death. At intensities up to approximately 6 W/cm^2 only a small reduction in cell survival was identified. However, over this threshold intensity the cell survival followed a negative linear slope with increasing intensity. At 10 W/cm^2 the cell surviving fraction was approximately 15 %. The cell killing was not induced by an apoptotic pathway but resulted in cell lysis, loss of membrane integrity and reduced clonogenic cell survival. Synergistic effects between HIFU and γ radiation existed, independent of the order of delivery even after long delay times such as 2 hours.

8.2 THE EFFECTS OF ACOUSTIC ENERGY ON ELECTRICAL ADMITTIVITY

High intensity ultrasound is often highly non-linear. Many applications not fully applicable today will in the future become possible when advanced feed forward and feed back regimes etc. are developed. Consequently, there exists a demand for relevant methods to monitor the target alteration. Our group have previously studied the secondary emission of acoustic energy from the target region to monitor the mechanical effect in the target region [1].

This study investigated the variation in in-vitro tissue admittivity after exposure to different kinds of acoustic radiation, namely extra corporeal shock wave lithotripsy (ESWL) and high intensity focused ultrasound (HIFU). The latter is carried out in both pulsed and continuous modes of delivery. A variation in tissue admittivity after acoustic irradiation may serve as a tool to monitor the degree of tissue alteration.

The electrical properties of tissue have been studied extensively since the middle of the 19th century with pioneer work by du Bois-Reymond, Fricke, Cole and others [76]. The early work was aimed at explaining, modelling and parameterising the complicated behaviour of tissue complex impedance. This work made it possible to use impedance measurements to characterise different tissues [77], detect pathological changes (both malignant and non-malignant) [78-83], and detect temperature changes [84]. Hence, it seems reasonable that also mechanical and thermal interaction with the tissue would induce permanent detectable changes in the electrical admittivity.

Before sonication of the samples the temperature and the admittivity of the specimens were measured. The admittivity was measured at 1 MHz with a specially made measuring probe, figure 21. This frequency is in the β -dispersion region where structural and capacitive changes of the cell membrane can be detected, chapter 3.2. The sample tissue was prime rib (beef) from animals sacrificed 1 day prior to the protocols. The size of the specimen was 1.3 g, (approx. 1 cm^3). The sample admittivity was measured 15-20 times and averaged to minimise the variation within each tissue sample.

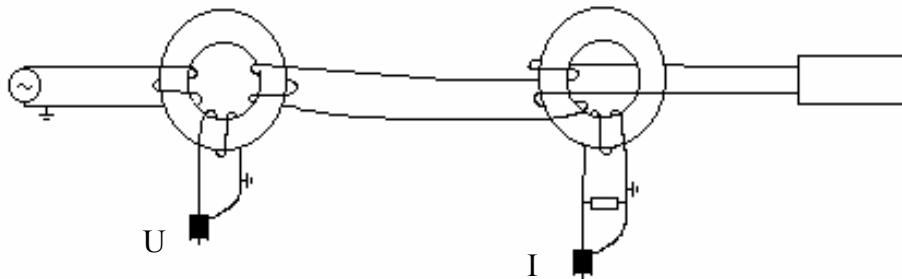


Figure 21. Overview of the used admittivity probe. The spherically shaped ($d = 1.3 \text{ mm}$) contact electrodes are placed 2.3 mm apart and mounted close to two ferrite-core transformers with included voltage and current measuring circuits.

During sonication each tissue sample was placed in a thin condom filled with isotone saline solution. Following sonication, identical temperature and admittivity measurements were carried out on the specimen. Care was taken to ensure that all measurements before and after the treatment were performed at the same temperature $\pm 0.5^\circ\text{C}$ ($17\text{-}22^\circ\text{C}$). The influence of the saline solution on the sample tissue was compensated for.

During the ESWL protocol 600 shock wave pulses were given at approximately 82 MPa . This protocol did not affect the temperature of the target tissue. The pulsed HIFU protocol consisted of $60 \mu\text{s}$ pulses containing sine bursts at 1.1 MHz . The passive period time was 100 ms , resulting in a duty-cycle factor of 6×10^{-4} . The Spatial Peak Temporal Peak (SPTP) intensity is assumed to be 31 kW/cm^2 giving a Spatial Peak

Temporal Average (SPTA) intensity of 19 W/cm². The pulsed exposure was sustained for 10 minutes. Temperature elevation was less than 1°C. The continuous protocol consisted of 1.1 MHz sine wave with an intensity adjusted to maintain a constant focal temperature of 44°C (Spatial peak intensity 72 W/cm²) and 80 °C (Spatial peak intensity 504 W/cm²) during 10 minutes.

Protocol	Before		After		Change %	
	Modulus	Phase	Modulus	Phase	Modulus	Phase
ESWL	0,567± 0,053 (n=11)	-7,540± 2,798 (n=11)	0,603± 0,067 (t=0,152)	-2,928± 1,401 (t=0,0002)	-----	61.2
HIFU pulsed	0,595± 0,050 (n=11)	-6,230± 1,827 (n=11)	0,611± 0,048 (t=0,055)	-2,463± 0,914 (t=0,0002)	-----	60.5
HIFU cont. 44°C	0,581± 0,041 (n=6)	-6,645± 2,198 (n=6)	0,579± 0,050 (t=0,946)	-3,289± 2,311 (t=0,004)	-----	50.5
HIFU cont. 80°C	0,623± 0,071 (n=6)	-5,761± 0,765 (n=6)	0,408± 0,057 (t=0,0007)	-1,715± 0,391 (t=0,0002)	-34.5	70.2

Table 3. Magnitude of admittivity and phase angle of impedivity at 1MHz before and after sonication of the tissue samples. All data are presented as mean with standard deviation including compensation for the saline deviation. Two sided paired student t-tests were performed to establish statistical significance. t<0.05 is considered significant.

The negative phase angle of impedivity significantly increased during all the protocols, table 3. We believe that this increase is caused by cell membrane disruption. Hober [85] showed that a red blood cell suspension lost its capacitance after disruption of the cell membranes. Furthermore, in-vitro measurements exclude the effects of vascularisation, i.e. temperature regulation, active changes in intra and extra- cellular fluids, and therefore primarily measure changes in the structure of the cell. The phase angle is thus an indicator of cell membrane status. The secondary emission from the cavitation bubbles during the HIFU and ESWL seems to disintegrate the cell membrane and increase the phase angle. During the continuous 80°C HIFU the cell membranes are also destroyed because of the elevated pressure associated with temperature rise and phase transformation. Our pulsed HIFU protocol can disrupt fibrin-fibrils of blood clots [6], indicating that the delivered energy with this HIFU regime is highly capable of destroying biological structures. The magnitude of admittivity decreased significantly only during continuous HIFU at 80 °C. This effect is caused by the elevated temperature and appears mainly due to coagulation, which decreases the ion mobility.

8.3 CONCLUSION AND FUTURE WORK

In conclusion both non-thermal and thermal effects seem to influence the phase angle of admittivity due to rupture of the cell membranes. Thermo therapy also influences the magnitude of admittivity, due to coagulation and protein denaturation. Hence, it seems feasible to use the electrical admittivity to monitor target alteration for both thermal and non-thermal acoustic protocols.

9 ACKNOWLEDGEMENTS

I would like to express my sincere gratitude to all those who made this PhD project possible. In particular I would to thank the following:

The gourmet gang at Comair for enlightening me in the fine arts of cooking and teaching me that quality is often better than quantity.

My Supervisor, Hans Wiksell for being the most brilliant technical mind I know and a good friend. I'm also grateful to you for giving me the opportunity to work in the fascinating field of medical engineering. Your contribution was of course vital for this work. I learned more from you about technical things and gadgets than anywhere else.

Technician Bo Lindström, for your assistance, friendship, encouragement and advice on many matters.

Peter Harge and Johan Thorell at VibraTech for financial support and for bringing your invaluable business know-how and enthusiasm into the projects.

Professor Håkan Elmquist, Division of Medical Engineering, Department of Laboratory Medicine, Karolinska Institute, for giving your support and for your invaluable help and encouragement during this project.

Associate Professor Hans Berglund, Department of Cardiology, Huddinge Hospital for invaluable linguistic guidance, training in the fine arts of writing scientific papers and help with the thrombus provocation study.

Professor Anders Eriksson, KTH Mechanics, Royal Institute of Technology for introducing me into the fascinating world of FEM analysis and for invaluable help and guidance with the FEM paper.

Associate Professor Bo Bergman, Urology Unit, Department of Surgical Science, Karolinska Hospital, for invaluable linguistic and scientific help with the TUMT article and for your encouragement and support.

Professor Gert Auer, Department of Oncology and Pathology, KI, for fruitful discussions.

Professor Lars-Ove Farnebo, Head of the Department of Surgical Science, Karolinska Institute, for comprehensive encouragement and support.

Helena Nässén, Head of administration, Department of Surgical Science, Karolinska Institute, for answering my many questions and invaluable help with complicated administration and formalities.

Urotherapist Kerstin Cronwall, Urology Unit, Karolinska Hospital, for your skilful work and care, the pleasant conversations we had during the TUMT treatments and for your enjoyable and cheerful personality.

NUTEK/VINNOVA especially CEO Per Eriksson and administrator Maj-Lis Ströman, for giving me the financial support to work on this project.

I would like to end this thesis by thanking my family, my girlfriend Kristin and all my friends.

Ma and Pa thank you for a wonderful childhood and interminable encouragement, love and support. Ma, many thanks for your proofreading of all my papers and this thesis. I suppose I have to thank Pa for the dominant mathematical gene that made this thesis possible.

Kristin thank you for being beautiful, lovable, encouraging and above all the best girlfriend in the world.

Finally, I would like to thank my friends for their support. I love you all!

10 REFERENCES

- [1] Westermark S. Modern therapeutic applications of acoustic and electromagnetic energy. Licentiate thesis, Karolinska Institute, Department of surgical sciences; 1999.
- [2] Lele PP. Thresholds and mechanisms of ultrasonic damage to "organised" animal tissue. In: Hazzard DG, Litz ML (eds). Symposium on biological effects and characterisations of ultrasonic sources. DHEW publication FDA 78-8048. United States Department of Health Education and welfare, Rockville, MD 1977: 224-239.
- [3] ter Haar GR, Stratford IJ. Evidence for a non-thermal effect of ultrasound. *Br J Cancer Suppl* 1982; 45; 172-5.
- [4] ter Haar GR, Daniels S. Evidence for ultrasonically induced cavitation in vivo. *Phys Med Biol* 1981; 26; 1145-9.
- [5] Gautherie M. Methods of external hyperthermic heating. Springer-Verlag, Berlin, Heidelberg 1990.
- [6] Westermark S, Wiksell H, Elmqvist H, Hultenby K, Berglund H. Effect of externally applied focused acoustic energy on clot disruption in vitro. *Clinical Science* 1999; 97; 67-71.
- [7] Kremkau FW. Cancer therapy with ultrasound: a historical review. *J Clin Ultrasound* 1979; 7; 287-300.
- [8] Lele PP. Production of deep focal lesions by focused ultrasound--current status. *Ultrasonics* 1967; 5; 105-12.
- [9] Fry FJ, Kossoff G, Eggleton RC, Dunn F. Threshold ultrasonic dosages for structural changes in the mammalian brain. *J Acoust Soc Am* 1970; 48; 1413-1417.
- [10] Marberger M. Editorial chapter. In: thermal tissue ablation. *European Urology* 1993; 23.S1; 3.
- [11] Madersbacher S, Kratzik C, Szabo N, Susani M, Vingers L, Marberger M. Tissue ablation in benign prostatic hyperplasia with high-intensity focused ultrasound. *Eur Urol* 1993; 23; 39-43.
- [12] Hynynen K. The threshold for thermally significant cavitation in dog's thigh muscle in vivo. *Ultrasound Med Biol* 1991; 17; 157-69.
- [13] ter Haar GR, Hopewell JW. Ultrasonic heating of mammalian tissues in vivo. *Br J Cancer Suppl* 1982; 45; 65-7.

- [14] Duck FA, Perkins MA. Amplitude-dependent losses in ultrasound exposure measurement. IEEE transactions on ultrasound, ferroelectrics and frequency control 1988: 35; 232-241.
- [15] Wiksell H. Effects of excitation methods on the attenuation of high intensity focused ultrasound in water. Phys Med 1995: 11; 43-49.
- [16] Kinn A-C, Wiksell H, Carbin BE, Ohlsén H. Experimental and clinical experiences with extra corporeal shock wave lithotripsy with Lithocut. J Endourol 1991: 5; 351-356.
- [17] Wiksell H. Development of a new ESWL-system with high stone fracturing power, low pain and low cost. Scand J Urol Nephrol 1992: 26; 19.
- [18] Kinn A-C, Andersson L, Carbin B-E, Ohlsen H, Skoog L, Wiksell H. Experimental and clinical experiences of Lithocut – a Swedish ESWL-apparatus. Scand Urol Nephrol 1992: 26; 19-20.
- [19] Grabe M, Kinn A-C, Alhgren G, Carbin B-E. Treatment of Renal and ureteral stones with Lithocut C-3000 Lithotripter. J Endourol 1992: 6; 403-406.
- [20] Daehlin L, Hellang M, Ulvik N-M. Shock wave Lithotripsy of urinary calculi with Lithocut C-3000 in a small center. Int urol Nephrol 1997: 29; 617-621.
- [21] Wiksell H, Kinn AC. Implications of cavitation phenomena for shot intervals in extracorporeal shock wave lithotripsy. Br J Urol. 1995: 75; 720-3.
- [22] Westermark S, Nelson E, Kinn A-C, Wiksell H. Effect of concentration of dissolved gases in the coupling medium on focal pressure in ESWL treatment. Phys Med 1998: 14; 51-53.
- [23] Westermark S, Nelson E, Kinn AC, Wiksell H. The impact of the geometry of the lithotripter aperture on fragmentation effect at extracorporeal shock wave lithotripsy treatment. Urol Res 1999: 27; 262-5.
- [24] An Internet resource for the calculation of the dielectric properties of body tissues in the frequency range 10 Hz - 100 GHz, <http://niremf.ifac.cnr.it/tissprop/>, ITALIAN NATIONAL RESEARCH COUNCIL, Institute for Applied Physics “Nello Carrara”, Florence (Italy).
- [25] Lopicque L. L'excitabilité en fonction de temps. Paris Les Presses Universitaires de France 1928.
- [26] Slager CJ, Schuurbijs JC, Oomen JA, Bom N. Electrical nerve and muscle stimulation by radio frequency surgery: role of direct current loops around the active electrode. IEEE Trans Biomed Eng 1993: 40; 182-187.

- [27] Lacourse JR, Miller WT 3rd, Vogt M, Selikowitz SM. Effect of high-frequency current on nerve and muscle tissue. *IEEE Trans Biomed Eng* 1985: 32; 82-86.
- [28] Gazelle S, Goldberg N, Solbiati L, Livraghi T. Tumor ablation with Radio-frequency energy. *Radiology* 2000: 217; 633-46.
- [29] Izzo F, Thomas R, Delrio P, Rinaldo M, Vallone P, DeChiara A, Botti G, D'Aiuto G, Cortino P, Curley SA. Radiofrequency ablation in patients with primary breast carcinoma. *Cancer* 2001: 92; 2036-44.
- [30] Livraghi T, Goldberg N, Monti F, Bizzini A, Lazzaroni S, Meloni F, Pellicano S, Solbiati L, Gazelle S. Saline-enhanced Radio Frequency Tissue Ablation in the Treatment of Liver Metastases. *Radiology* 1997: 202; 205-10.
- [31] Goldberg S, Gazelle S, Solbiati L, Rittman W, Mueller P. Radiofrequency Tissue Ablation: Increased Lesion Diameter with a Perfusion Electrode. *Acad Radiol* 1996: 3; 636-44.
- [32] Kyle UG, Piccoli A, Pichard C. Body composition measurements: interpretation finally made easy for clinically use. *Curr Opin Nutr Metab Care* 2003: 6; 387-393.
- [33] Brown BH. Electrical impedance tomography (EIT): a review. *J Med Eng Technol* 2003: 27; 97-108.
- [34] Åberg P, Nicander I, Holmgren U, Geladi P, Ollmar S. Assessment of skin lesions and skin cancer using simple electrical impedance indices. *Skin Res Technol* 2003: 9; 257-261.
- [35] Åberg P, Nicander I, Hamsson J, Geladi P, Holmgren U, Ollmar S. Skin cancer identification using multi-frequency electrical impedance – a potential screening tool. *IEEE Trans Biomed Eng* 2004: in press.
- [36] Åberg P, Geladi P, Nicander I, Hamsson J, Holmgren U, Ollmar S. Non-invasive and microinvasive electrical impedance spectra of skin cancer – a comparison between two techniques. *Skin Res Technol* in press.
- [37] Jossinet J, Marry E, Montalibet A. Electrical impedance endotomography: imaging tissue from inside. *IEEE Trans Med Imaging* 2002: 21; 560-5.
- [38] Chang I. Finite Element Analysis of Hepatic Radiofrequency Ablation Probes using Temperature-Dependent Electrical Conductivity. *BioMedical Engineering Online* 2003: 2; 12.
- [39] Miller RC, Connor WG, Heusinkveld RS, Boone ML. Prospects for hyperthermia in human cancer therapy. Part I: hyperthermic effects in man and spontaneous animal tumors. *Radiology* 1977: 123; 489-95.

- [40] Dewey WC, Hopwood LE, Sapareto SA, Gerweck LE. Cellular responses to combinations of hyperthermia and radiation. *Radiology* 197; 123; 463-74.
- [41] Hall EJ. *Radiobiology for the radiologist* 2:nd ed, Harper and Row, 1978, pp 325-328.
- [42] Haemmerich D, Chachati L, Wright AS, Mahvi DM, Lee FT Jr, Webster JG. Hepatic radiofrequency ablation with internally cooled probes: effect of coolant temperature on lesion size. *IEEE Trans Biomed Eng* 2003; 50; 493-500.
- [43] R. D. Cook, D. S. Malkus, M. E. Plesha, R. J. Witt, *Concepts and Applications of Finite Element Analysis*. 4th ed., Wiley, 2002.
- [44] O. C. Zienkiewicz, R. L Taylor, *The Finite Element Method*. Volume 1: The basis. 5th ed., Butterworth-Heinemann, 2000.
- [45] Mebust WK, Holtgrewe HL, Cockett ATK, Peters PC. Transurethral prostatectomy: immediate and post-operative complications. A co-operative study of 13 participating institutions evaluating 3885 patients. *J Urol* 1989; 141; 243-247.
- [46] Bolmsjö M, Wagrell L, Hallin A, Eliasson T, Erlandsson B-E, Mattiasson A. The heat is on - but how? A comparison of TUMT devices. *Br J Urol* 1996; 78; 564-72.
- [47] Nordenstam G, Aspelin P, Isberg B, Svensson L, Hallin A, Berlin T. Effect of transurethral microwave thermotherapy. An evaluation with MR imaging. *Acta Radiol* 1996; 37; 933-6.
- [48] Devonec M, Carter SStC, Tubaro A, de la Rosette J, Höfner K, Dahlstrand C. Microwave therapy. *Current Opinion in Urology* 1995; 5; 3-9.
- [49] Ogden CW, Reddy P, Johnson H, Ramsay JWA, Carter SStC. Sham versus transurethral microwave thermotherapy in patients with symptoms of benign prostatic bladder outflow obstruction. *Lancet* 1993; 341;14-7.
- [50] De Wildt MJAM, Hubregtse M, Ogden C, Carter SStC, Debruyne FMJ, de la Rosette JJMCH. A 12-month study of the placebo effects in transurethral microwave thermotherapy. *Br J Urol* 1996; 77; 221-7.
- [51] D'Ancona F, Francisca E, Hendriks J, Debruyne F, de la Rosette J. How to select patients for high-energy transurethral microwave thermotherapy. *Urology* 1999; 53; 111-7.
- [52] Brehmer M, Wiksell H, Kinn A-C. Sham treatment compared with 30 or 60 minutes of thermotherapy for benign prostatic hyperplasia: a randomised study. *Br J Urol* 1999; 84; 292-6.

- [53] Brehmer M, Hilliges M, Kinn A-C. Denervation of periurethral prostatic tissue by transurethral microwave thermotherapy. *Scand J Urol Nephrol* 2000; 34; 42-5.
- [54] Bergman B, Litvinenko AG, Sandstedt B, Wiksell H. Histopathological findings after transurethral microwave therapy of benign prostatic hyperplasia. 1996; 30; Suppl 177.
- [55] Bergman B, Wiksell H. Shortened treatment time in transurethral microwave thermotherapy of benign prostatic hyperplasia: follow-up after ECP. *Scand J Urol Nephrol* 1993; 24; 155.
- [56] Brehmer M, Kinn A-C. Transurethral Microwave Thermotherapy for benign prostatic hyperplasia: Subjective response and urodynamic changes. *Scand J Urol Nephrol* 1996; 30; 307-11.
- [57] Hallin A, Berlin T. Transurethral Microwave Thermotherapy of Benign Prostatic Hyperplasia: Do any pretreatment conditions predict the result? *Eur Urol* 1996; 30; 429-36.
- [58] Singletary S. Minimally invasive techniques in breast cancer treatment. *Semin Surg Oncol* 2001; 20; 246-250.
- [59] Hall-Craggs MA, Vaidya JS. Minimally invasive therapy for the treatment of breast tumours. *Eur J Radiol* 2002; 42; 52-57.
- [60] Shultz I, Ekstrand V, Sandstedt B, Grundström H, Rotstein S, Wiksell H. Bröstkancer kan destrueras in-vitro genom högfrekvensvärmning. 8:e kirurgveckan i Karlstad 2003.
- [61] Jossinet J. Variability of impedivity in normal and pathological breast tissue. *Med Biol Eng comput* 1996; 34; 346-350.
- [62] Graham SJ, Chen L, Leitch M, Peters RD, Bronskill MJ, Foster FS, Henkelman RM, Plewes DB. Quantifying tissue damage due to focused ultrasound heating observed by MRI. *Magn Reson Med* 1999; 41; 321-28.
- [63] Saniabadi AR, Umemura K, Matsumoto N, Sakuma S, Nakashima M. Vessel wall injury and arterial thrombosis induced by a photochemical reaction. *Thromb Haemost* 1995; 73; 868-72.
- [64] Wang S, Garner DJ, Romano M, Peng SK, Goldberg SL, French WJ. A simple, reproducible animal model of arterial occlusion with mixed thrombus. *J Thromb Thrombolysis* 1996; 3; 337-41.
- [65] Weidenbach H, Sedlarik K, Reimann G, Wilde J. Light and electron microscopy studies on experimental arterial thrombosis in dwarf swine. *Z Exper Chirurg* 1978; 11; 230-7.

- [66] Kornowski R, Glikson M, Ohad D, Varda-Bloom N, Battler A. Electrical injury in the femoral artery of rabbits as a model for arterial thrombosis: a pilot study. *Angiology* 1994; 45; 295-300.
- [67] Guarini S. A highly reproducible model of arterial thrombosis in rats. *J Pharmacol Toxicol Methods* 1996; 35; 101-5.
- [68] Schumacher WA, Steinbacher T.E, Megill JR, Durham SK. A ferret model of electrical-induction of arterial thrombosis that is sensitive to aspirin. *J Pharmacol Toxicol Methods* 1996; 35; 3-10.
- [69] Sedlarik K, Schilling B, Seelig G. The electrically induced thrombosis in the arteria femoralis of pig as a model for in-vivo studies. *Z Exp Chirurg* 1977; 10; 23-9.
- [70] Friendman MF, Van der Bovenkamp GJ. The pathogenesis of a coronary thrombus. *Am J Pathol* 1966; 48; 19-44.
- [71] Andre P, Bal dit Sollier C, Bonneau M, Pignaud G, Hainaud P, Azzam K, Drouet L. Which experimental model to choose to study arterial thrombosis and evaluate potentially useful therapeutics? *Haemostasis* 1996; 26; 55-69.
- [72] Goodman SL. Sheep, pig, and human platelet-material interactions with model cardiovascular biomaterials. *J Biomed Mater Res* 1999; 45; 240-250.
- [73] Softeland E, Framstad T, Thorsen T, Holmsen H. Porcine platelets in vitro and in vivo studies: relevance to human thrombosis research. *Eur.J.Haematol.* 1992; 49; 161-73.
- [74] Brinkhous KM. Animal models: importance in research on hemorrhage and thrombosis. *Adv Exp Med Biol* 1978; 102; 123-33.
- [75] Jernberg A, Hedlöf I, Heiden T, Ekstrand V, Wiksell H, Brahme A, Lewensohn R, Edgren M. Cell death induced by high-intensity ultrasound alone and in combination with γ radiation in a human small cell lung carcinoma cell line. Manuscript under development.
- [76] MCAdams ET, Jossinet J. Tissue impedance: a historical overview. *Physiol Meas* 1995; 16; A1-A13.
- [77] Rigaud B, Hamzoui L, Frikha MR, Chauveau N, Morucci JP. In vitro tissue characterization and modelling using electrical impedance measurements in the 100 Hz-10 MHz frequency range. *Physiol Meas* 1995; 16; A15-A21.
- [78] Jossinet J. Variability in normal and pathological breast tissue. *Med & Biol Eng & Comput* 1996; 34; 346-50.
- [79] Blad B, Wendel P, Jönsson M, Lindström K. An electrical impedance index to distinguish between normal and cancerous tissues. *J Med Eng & Technol* 1999; 23; 57-62.

- [80] Morimoto T, Kimura S et al. A study of the electrical bio-impedance of tumours. *J Investing Surg* 1993; 6; 25-32.
- [81] Fricke H, Morse S. The electric capacity of tumours of the breast. *J Cancer Res* 1926; 10; 340-76.
- [82] Surowiec AJ, Stuchly SS, Barr JR, Swarup A. Dielectric properties of breast carcinoma and the surrounding tissues. *IEEE Trans* 1988; BME-35; 257-63.
- [83] Konishi Y, Morimoto T, Kinouchi Y, Iritani T, Monden Y. Electrical properties of extracted rat liver tissue. *Res Exp Med (Berl)* 1995; 195; 183-92.
- [84] Gersing E. Monitoring temperature-induced changes in tissue during hyperthermia by impedance methods. *Ann N Y Acad Sci* 1999; 873; 13-20.
- [85] Hober R. Messungen der innern Leitfähigkeit von zellen III. *Arch Ges Physiol* 1913; 150; 15-145.